ANL-HEP-TR-92-59
STAR NOTE #77

Estimates of Rates and Errors for Measurements of Direct-γ and Direct-γ + Jet Production by Polarized Protons at RHIC*

M. E. Beddo, H. Spinka, and D. G. Underwood

High Energy Physics Division
Argonne National Laboratory
Argonne, Illinois 60439

August 14, 1992

Abstract

Studies of inclusive direct-γ production by pp interactions at RHIC energies were performed. Rates and the associated uncertainties on spin-spin observables for this process were computed for the planned PHENIX and STAR detectors at energies between $\sqrt{s} = 50$ and 500 GeV. Also, rates were computed for direct-γ + jet production for the STAR detector. The goal was to study the gluon spin distribution functions with such measurements. Recommendations concerning the electromagnetic calorimeter design and the need for an endcap calorimeter for STAR are made.

*Work supported by the U.S. Department of Energy, Division of High Energy Physics, Contract W-31-109-ENG-38.

Physics Motivation

Measurements of deep inelastic polarized electron and muon scattering from polarized proton targets at SLAC[1–3] and CERN[4] have been interpreted in terms of the fraction of the proton's spin carried by the quarks. In these experiments, both the beam leptons and the target protons are polarized along the beam direction (longitudinally). The results were initially interpreted to suggest that the quarks carry a small fraction of the net helicity of the proton.[4,5] A large number of theoretical papers have been written to understand this surprising conclusion, and the present situation is summarized in Ref. 6. It should be noted that at small x, the experimental values from the deep inelastic scattering spin measurements differ by about three standard deviations from the values predicted before the experiment.

The proton helicity is the sum of contributions from quarks, (sea) antiquarks, gluons, and orbital angular momentum. The quark contribution is most easily obtained from deep inelastic lepton scattering, and the antiquark contribution from measurements of "massive" muon pairs from pp interactions (Drell-Yan).[7–12] On the other hand, the gluon contribution to the proton helicity can be derived from inclusive direct-γ[13–17] or jet[18–20] production using longitudinally-polarized protons scattering from longitudinally-polarized protons. This report studies the kinematics and rates for direct-γ production with a goal to obtain information on the gluon contribution to the proton helicity.

The two dominant subprocesses contributing to direct-γ production are the Compton (q g $\rightarrow \gamma$ q), and the annihilation (q $\overline{\text{q}} \rightarrow \gamma$ g) subprocesses.[21–23] In both cases, the final state involves a direct-γ and a jet (from the outgoing quark or gluon). The Compton subprocess is the larger one in pp interactions, since there are no valence antiquarks in the proton. Detailed calculations[23] indicate that the annihilation and Compton subprocesses represent about 70-80 percent of the cross section in the RHIC energy range, with essentially the rest from Bremsstrahlung. The ratio of the Compton to the annihilation cross section for typical P_T values is calculated to be larger than 5.

Since quark structure functions are known from deep inelastic lepton scattering, direct-γ + jet measurements with unpolarized proton beams have been used in the past[24] to obtain information on the (unpolarized) gluon structure function. Likewise, similar experiments with polarized beams will give information on the x-dependence of the polarized gluon structure function.

This report first considers some theoretical background and the relevant kinematic regions for direct-γ and jet detection. Next, cross sections for direct-γ and π^0 production are estimated using the expected luminosity from the RHIC accelerator. This is followed by discussions of several experimental methods to measure direct-γ production, including fine segmentation, a preconvertor, and a shower maximum detector. For these methods, rates and uncertainties on spin-spin observables such as A_{LL} are estimated for the PHENIX and STAR

detectors. Next, the kinematics and rates for direct-γ + jet detection in STAR are evaluated. Finally, a set of conclusions are listed based on these studies.

Theoretical Background

In the unpolarized case, inclusive direct-γ production data have been used to extract information on the gluon structure function $G(x)$ in the proton.[21,25–29] Under the assumption that the Compton subprocess is the only contribution to the cross section, then

$$\frac{d^4\sigma(pp \rightarrow \gamma + Jet + X)}{d(P_T^2)d\phi dy_\gamma dy_{Jet}} \propto \sum_f q_f(x_a)G(x_b)\frac{d\sigma}{d\hat{t}}(q_f g \rightarrow \gamma q), \tag{1}$$

where y_γ and y_{Jet} are the rapidities of the direct-γ and jet, respectively. The $q_i(x)$ are the quark structure functions in the proton (u(x), d(x), etc. for u,d,... quarks) determined from deep inelastic scattering,[30] and the momentum fractions x_a and x_b (x = $2P_T/\sqrt{s}$) can be related to the rapidities y_γ and y_{Jet}. The parton level cross sections $d\sigma/d\hat{t}$ can be calculated from perturbative QCD when the process is a hard scattering.[21] For the purposes of this paper, the onset of hard scattering will be assumed to correspond to P_T = 10 GeV/c.

A number of corrections need to be applied to the simple relation above, corresponding to the annihilation and higher order subprocesses, as well as Bremsstrahlung effects.[21,23,31] In addition, there are corrections caused by isolation cuts on the experimental data,[32] and other effects that must be included in the calculations (k_T smearing, soft gluons, γ fragmentation function, ...). Nevertheless, the gluon structure function has been determined as a function of x from inclusive direct-γ + jet experimental data from the ISR.[24] Typical spin-averaged valence u-quark,sea $\bar{u}$-quark, and gluon structure functions in the proton[30] are shown in Fig. 1.

The structure functions $q_i(x)$ must be sizeable in order to obtain sufficient rate and sensitivity to the gluon structure function. Then "high" rates correspond to large $G(x)$, and "low" rates to small $G(x)$. From Fig. 1 it can be seen that the higher rates will correspond to x of the quark in the range 0.02 - 0.5, and to x of the gluons $\leq$ 0.4. In addition to having large $q(x)$, the parton level cross section $d\sigma/d\hat{t}$ must also be large. Figure 2 shows a plot of the Compton and annihilation cross sections as a function of c.m. scattering angle. It can be seen that the cross section will be the largest at very forward c.m. angles and relatively constant over the remaining angular range.

The single inclusive direct-γ production cross section is an integral over the γ + jet cross section,

$$\begin{aligned} E_\gamma \frac{d^3\sigma(pp \to \gamma X)}{dP_\gamma^3} &= 2\frac{d^3\sigma}{d(P_T^2)d\phi dy_\gamma} \\ &\propto \int dy_{jet}(x_a, x_b) \sum_f q_f(x_a) G(x_b) \frac{d\sigma}{d\hat{t}}(q_f g \to \gamma q). \end{aligned} \quad (2)$$

In this case it is difficult to extract information on the x-dependence of $G(x)$. On the other hand, most of the experimental data reported in the literature are for the single inclusive cross section ($pp \to \gamma + X$).

For the case with spin, similar considerations apply. The analogy of the unpolarized structure functions are the spin dependent structure functions

$$\begin{aligned} \Delta u(x) &= [u_+^+(x) - u_-^+(x)]/2, \\ \Delta d(x) &= [d_+^+(x) - d_-^+(x)]/2, \\ \Delta G(x) &= [G_+^+(x) - G_-^+(x)]/2, \\ &etc., \end{aligned} \quad (3)$$

with subscripts corresponding to + and – helicities of the partons, and the superscript to the proton helicity. Similarly, the spin-dependent cross sections are

$$\Delta\sigma = [\sigma(++) + \sigma(--) - \sigma(+-) - \sigma(-+)]/4. \quad (4)$$

In contrast, the spin-averaged quantities are

$$\begin{aligned} u(x) &= [u_+^+(x) + u_-^+(x)]/2, \\ d(x) &= [d_+^+(x) + d_-^+(x)]/2, \\ G(x) &= [G_+^+(x) + G_-^+(x)]/2, \\ \sigma &= [\sigma(++) + \sigma(--) + \sigma(+-) + \sigma(-+)]/4. \end{aligned} \quad (5)$$

The following relations hold for the spin-dependent structure functions of the proton (by parity conservation):

$$\begin{aligned} u_+^-(x) &= u_-^+(x), \\ u_-^-(x) &= u_+^+(x), \\ d_+^-(x) &= d_-^+(x), \\ d_-^-(x) &= d_+^+(x), \\ G_+^-(x) &= G_-^+(x), \\ G_-^-(x) &= G_+^+(x), \\ &etc. \end{aligned} \quad (6)$$

The contribution to the direct-γ + jet inclusive cross section by the Compton subprocess is given in terms of these quantities by

$$\frac{d^4\Delta\sigma(pp \to \gamma + Jet + X)}{d(P_T^2)d\phi dy_\gamma dy_{Jet}} \propto \sum_f \Delta q_f(x_a)\Delta G(x_b)\frac{d\Delta\sigma}{d\hat{t}}(q_f g \to \gamma q), \tag{7}$$

and for the single inclusive direct-γ production cross section by

$$E_\gamma \frac{d^3\Delta\sigma(pp \to \gamma X)}{dP_\gamma^3} \propto \int dy_{jet}(x_a, x_b) \sum_f \Delta q_f(x_a)\Delta G(x_b)\frac{d\Delta\sigma}{d\hat{t}}(q_f g \to \gamma q). \tag{8}$$

Note that these equations follow from the definitions above as follows:

$$\begin{aligned}
\frac{d^4\Delta\sigma}{dP_T^2 dy_\gamma dy_{Jet}} &= \frac{1}{4}\frac{d^4\sigma(++)}{dP_T^2 dy_\gamma dy_{Jet}} + \frac{1}{4}\frac{d^4\sigma(--)}{dP_T^2 dy_\gamma dy_{Jet}} - \frac{1}{4}\frac{d^4\sigma(+-)}{dP_T^2 dy_\gamma dy_{Jet}} \\
&\quad - \frac{1}{4}\frac{d^4\sigma(-+)}{dP_T^2 dy_\gamma dy_{Jet}} \\
&\propto \frac{1}{16}\sum_f \left[q_{f+}^+ G_+^+ \frac{d\sigma(++)}{d\hat{t}} + q_{f+}^+ G_-^+ \frac{d\sigma(+-)}{d\hat{t}} + q_{f-}^+ G_+^+ \frac{d\sigma(-+)}{d\hat{t}} \right. \\
&\quad \left. + q_{f-}^+ G_-^+ \frac{d\sigma(--)}{d\hat{t}} \right] \\
&\quad + \frac{1}{16}\sum_f \left[q_{f+}^- G_+^- \frac{d\sigma(++)}{d\hat{t}} + q_{f+}^- G_-^- \frac{d\sigma(+-)}{d\hat{t}} + q_{f-}^- G_+^- \frac{d\sigma(-+)}{d\hat{t}} \right. \\
&\quad \left. + q_{f-}^- G_-^- \frac{d\sigma(--)}{d\hat{t}} \right] - \cdots \\
&\propto \frac{1}{16}\sum_f (q_{f+}^+ - q_{f+}^-)[(G_+^+ - G_+^-)\frac{d\sigma(++)}{d\hat{t}} + (G_-^+ - G_-^-)\frac{d\sigma(+-)}{d\hat{t}}] \\
&\quad + \frac{1}{16}\sum_f (q_{f-}^+ - q_{f-}^-)[(G_+^+ - G_+^-)\frac{d\sigma(-+)}{d\hat{t}} + (G_-^+ - G_-^-)\frac{d\sigma(--)}{d\hat{t}}].
\end{aligned} \tag{9}$$

Making use of Eq. 6 gives,

$$\begin{aligned}
\frac{d^4\Delta\sigma}{d(P_T^2)d\phi dy_\gamma dy_{Jet}} &\propto \frac{1}{16}\sum_f (q_{f+}^+ - q_{f-}^+) \cdot (G_+^+ - G_-^+) \cdot [\frac{d\sigma(++)}{d\hat{t}} + \frac{d\sigma(--)}{d\hat{t}} \\
&\quad - \frac{d\sigma(+-)}{d\hat{t}} - \frac{d\sigma(-+)}{d\hat{t}}].
\end{aligned} \tag{10}$$

This equation reduces to Eq. 7 from the definitions in Eq. 3. In a similar fashion, the spin-dependent structure functions can be combined for the case with unpolarized beams to yield Eq. 1.

Information on the quark spin distribution functions is obtained from deep inelastic lepton scattering experiments at SLAC[1–3] and CERN.[4] The experimental measurements with polarized leptons and polarized protons in helicity states are most closely related to the quantity[15]

$$g_1(x,Q^2) = \sum_f \frac{e_f^2}{2}[\Delta q_f(x,Q^2) + \Delta\overline{q_f}(x,Q^2) - \frac{\alpha_s(Q^2)}{2\pi}\int_x^1 F(x,y)\Delta G(y,Q^2)dy], \quad (11)$$

where α_s is the strong coupling constant and e_f is the charge of the quark with flavor f. The function F is calculable in terms of $O(\alpha_s)$ corrections to the lowest-order diagrams, and it is dependent on the renormalization scheme. The experimental results are shown in Fig. 3,[4,5] and they suggest that the up-quarks are aligned with large probability along the proton's helicity direction for $x \sim 0.2$ to 0.6.

The integral of the data in Fig. 3 over x can be related to the net fraction of the proton's helicity carried by partons (in the k_T-cutoff scheme) as[33,34]

$$2\int_0^1 g_1(x,Q^2)dx = \frac{4}{9}\langle\Delta u\rangle + \frac{1}{9}\langle\Delta d\rangle + \frac{1}{9}\langle\Delta s\rangle - (\frac{4}{9}+\frac{1}{9}+\frac{1}{9})\frac{\alpha_s(Q^2)}{2\pi}\langle\Delta G(Q^2)\rangle, \quad (12)$$

where

$$\Delta u = \int_0^1 [\Delta u(x,Q^2) + \Delta\overline{u}(x,Q^2)],$$
$$\Delta d = \int_0^1 [\Delta d(x,Q^2) + \Delta\overline{d}(x,Q^2)],$$
$$\Delta s = \int_0^1 [\Delta s(x,Q^2) + \Delta\overline{s}(x,Q^2)], \quad (13)$$

are the fractions of the proton's helicity carried by u-, d-, and s-quarks, respectively, and

$$\langle\Delta G(Q^2)\rangle = \int_0^1 dx\Delta G(x,Q^2) \quad (14)$$

is the fraction carried by gluons. The integral in Eq. 12 plus information from Bjorken's sum rule[35] and semileptonic decays of hyperons,[36] allow the determination of individual quantities

$$\langle\Delta q_f(Q^2)\rangle - \frac{\alpha_s(Q^2)}{2\pi}\langle\Delta G(Q^2)\rangle \quad (15)$$

as well as the sum

$$\sum_f [\langle \Delta q_f \rangle - \frac{\alpha_s(Q^2)}{2\pi} \langle \Delta G(Q^2) \rangle] \simeq 0. \tag{16}$$

Initially, the presence of the ΔG terms in Eqs. 12 and 15 was not appreciated, and the small experimental value for the previous equation was interpreted to indicate that the net helicity carried by the quarks in the proton was nearly zero. This interpretation led to many theoretical papers attempting to explain such a surprising result. It is now apparent from Eq. 15 that a knowledge of $\Delta G(x)$ and $\langle \Delta G \rangle$ will be required to determine the fraction of the proton helicity carried by quarks. However, it was shown by Bodwin and Qui[37] that the magnitude of the hard gluonic contribution to $\int g_1(x)dx$ is dependent on the factorization convention chosen in defining $\Delta q(x)$. The choice of factorization scheme does not affect $g_1(x)$, $\int g_1(x)dx$, cross sections, or $\Delta G(x)$. However, it does change the function F in Eq. 11. In the $\overline{\rm MS}$ factorization scheme, the terms proportional to $\langle \Delta G \rangle$ vanish in Eqs. 12, 15, 16, and $\Delta q_{\overline{MS}} = \Delta q - \frac{\alpha_s}{2\pi} \Delta G$.

This note describes the use of inclusive direct-γ and direct- γ + jet production measurements with longitudinally-polarized protons incident on longitudinally-polarized protons to obtain information about $\Delta G(x)$ and $\langle \Delta G \rangle$. A number of theoretical predictions of spin effects in this process have been made in the past.[13–17] High-energy inclusive spin predictions are often given for the quantity,

$$A_{LL} = (E\frac{d^3\Delta\sigma}{dP^3})/(E\frac{d^3\sigma}{dP^3}), \tag{17}$$

since such asymmetries are usually measured in spin experiments. An identical formula applies to processes such as $pp \rightarrow \gamma + Jet + X$. Many systematic effects, such as detector efficiencies, absolute luminosity, etc. cancel in A_{LL}. Some of these systematic effects were particularly troublesome for past experiments with solid state polarized targets that contain substantial fractions of nonhydrogen background nuclei. These effects may be less of a problem with colliding proton beams, since they do not have the background nuclei present. In any case, uncertainties (δA_{LL}) on A_{LL} are estimated in this paper.

As in the unpolarized case, good sensitivity to $\Delta G(x)$ requires both $\Delta q(x)$ and $d\Delta\sigma/d\hat{t}$ to be large. The first condition can be met when x of the quark is larger than 0.2 to 0.3 using Fig. 3. At these larger x values, the gluon and sea antiquark structure functions are expected to be very small and to contribute little to $g_1(x)$ in Eq. 11, so that the valence quark terms dominate. Thus, the large $g_1(x)$ for $x > 0.2$ to 0.3 suggests that $\Delta u(x) + \Delta d(x)$ are large. The parton level cross sections $d\Delta\sigma/d\hat{t}$ are shown in Fig. 2, and are largest for forward c.m. angles for the Compton subprocess.

Parameterization of Cross Sections for Inclusive π^0 and Direct-γ Production

In order to make first order estimates of rates, analytical approximations to the invariant cross sections for inclusive π^0 and direct-γ production were fit to existing data. The results were then interpolated to the energies and P_T ranges of interest at RHIC. Finally, rates and the uncertainties on A_{LL} for inclusive direct-γ production were estimated for an ideal detector.

There are a number of experimental measurements of the single inclusive direct-γ production cross sections in pp and $p\overline{p}$ interactions.[38–45] Results from earlier experiments are summarized in Ref. 15. Some measurements on nuclear targets[46–48] have also been performed, and cross sections per nucleon will be assumed to be the same as for pp interactions. In order to estimate rates for particular P_T ranges, these data were fit with an exponential

$$E\frac{d^3\sigma}{dp^3} = B\,\exp\left(-bP_T\right), \tag{18}$$

and the results of the fits are summarized in Tables 1 and 2 and Fig. 4. Note that the $\overline{p}p \rightarrow \gamma X$ cross sections are expected to be somewhat (about a factor of 1.3) larger than for $pp \rightarrow \gamma X$.[23] While the Compton subprocess has the same cross section for both reactions, the annihilation subprocess cross section is much larger for $\overline{p}p$ than for pp interactions due to the presence of valence antiquarks in the antiproton.

When Eq. 18 is integrated for $\Delta\phi = 2\pi$ and $|\eta| < \Delta\eta/2$, the cross section for transverse momentum above P_T is found to be

$$\sigma_\gamma = \frac{2\pi B\Delta\eta}{b^2}(1+bP_T)\exp\left(-bP_T\right). \tag{19}$$

Note $d^3P/E = P_T dP_T d\eta d\phi$, and the cross section was assumed to be approximately independent of η over the range $-\Delta\eta/2$ to $\Delta\eta/2$. The cross section σ_γ for $P_T > 10$ GeV/c and $\Delta\eta = 2$ as a function of $\sqrt{s}$ is given in Fig. 5 from the fits to the experimental data.[38–48] The $\overline{p}p \rightarrow \gamma X$ cross sections have been reduced by a factor of 1.3 as noted before. The inclusive direct-γ production cross section for $P_T > 10$ GeV/c is seen to rise steeply with increasing $\sqrt{s}$.

For purposes of comparison in this paper, rates and estimated uncertainties for A_{LL} will be computed at $\sqrt{s} = 200$ GeV for various detector configurations. The inclusive direct-γ production cross section at $\sqrt{s}$ will be taken from a fit to the estimated cross section[49] for P_T between 5 and 12 GeV/c. This fit gives $B = 4.0\times10^4$ pb/GeV^2/c^3 and $b = 0.87$ /GeV/c from Eq. 18, which corresponds to $Ed^3\sigma/dP^3(P_T = 10\,\mathrm{GeV/c}) = 6.7$ pb/GeV^2/c^3, and $\sigma_\gamma = 1080$ pb for $\Delta\eta = 2$ and $P_T = 10 - 20$ GeV/c from Eq. 19. The fit parameters are seen to follow the trends of the experimental data shown in Figs. 4 and 5, although the cross section may be underestimated beyond $P_T = 12$ GeV/c.

The inclusive π^0 production cross section, by contrast, is considerably larger. It was assumed to be approximately equal to the inclusive charged-hadron production cross section as parameterized by UA1[50]:

$$E_\pi \frac{d^3\sigma}{dP_\pi^3} = \frac{A}{(1 + P_T/p_0)^N}, \tag{20}$$

The coefficients A, N, and p_0 are given in Tables 3, 4 and 5 and Fig. 6 from fits to a variety of experimental data.[42,50–55] With the same assumptions as before, the cross section for inclusive π^0 production for $\Delta\phi = 2\pi$, $|\eta| < \Delta\eta/2$, and transverse momentum larger than P_T is given by

$$\sigma_{\pi^0} = \frac{2\pi A p_0^2 \Delta\eta}{(N-1)(N-2)} \frac{(1 + (N-1)P_T/p_0)}{(1 + P_T/p_0)^{N-1}}. \tag{21}$$

At $\sqrt{s} = 200$ GeV, using the parameters fit to the UA1 results from Table 5, the cross section for $\Delta\eta = 2$ and $P_T = 10 - 20$ GeV/c is $\sigma_{\pi^0} = 5170$ pb $\simeq 5\sigma_\gamma$. The cross section from the fits for $P_T > 10$ GeV/c and $\Delta\eta = 2$ as a function of $\sqrt{s}$ are also plotted in Fig. 5, and this cross section also rises steeply with increasing $\sqrt{s}$.

The interpolated cross sections from Fig. 5 can be used to estimate uncertainties in $A_{LL}(pp \to \gamma X)$ for an ideal detector. A one month experiment with 100% operating efficiency will be assumed ($\Delta t \simeq 2.59 \times 10^6$ sec). Two values for the luminosity will be considered, the nominal or "design" RHIC luminosity, and the enhanced or high luminosity option;[56–58] see Fig. 7. Numerical values at $\sqrt{s} = 100, 200$, and 500 GeV are given in Table 6 assuming $\Delta\phi = 2\pi$, $\Delta\eta = 2$, and $P_T = 10 - 20$ GeV/c. The number of events N_γ is $L\sigma_\gamma \Delta t$, and the uncertainty on A_{LL} will be

$$\delta A_{LL} = \frac{1}{P_B^2} \cdot \frac{1}{\sqrt{N_\gamma}} \cdot \left[1 - (P_B^2 A_{LL})^2\right]^{\frac{1}{2}} \leq \frac{1}{P_B^2} \frac{1}{\sqrt{N_\gamma}}, \tag{22}$$

where P_B is the beam polarization, which is taken to be the same for the two colliding proton beams. From Table 6 it can be seen that the rate is quite low and δA_{LL} is relatively large for $\sqrt{s} = 100$ GeV at the design luminosity, but that the rates are reasonable for $\sqrt{s} = 200$ and 500 GeV, especially with the high luminosity option. The improved rates at higher $\sqrt{s}$ are the consequence of both the rapidly rising cross section σ_γ and the improved luminosity.

Note that theoretical predictions with different assumptions for $\Delta G(x)$ typically have differences on the order of $\Delta A_{LL} \sim 0.05$ in this kinematic region. For comparisons in this paper, $\sqrt{s} = 200$ GeV, $\Delta\eta = 2$, $\Delta\phi = 2\pi$, and $P_T = 10 - 20$ GeV/c with the design luminosity will be taken to be "standard conditions." For this case, the uncertainty for an ideal detector will be

$$\delta A_{LL} \leq \frac{1}{P_B^2}(0.008/\sqrt{\text{month}}) \tag{23}$$

On this basis alone a direct-γ spin-spin experiment will give important information on ΔG given a suitable EM calorimeter/detection system and reasonable beam polarizations.

For comparison, direct-γ events were generated using the ISAJET Monte Carlo code. EHLQ set # 2 structure functions[59] were used in this code. These events indicated an integrated cross section of $\sigma_\gamma \sim 820$ pb at $\sqrt{s} = 200$ GeV, $P_T = 10 - 20$ GeV/c, $\Delta\phi = 2\pi$, and $\Delta\eta = 2$. This agrees within about 30% with the estimate above. Figure 8 shows the inclusive direct-γ/jet production cross section used by ISAJET, and Table 7 shows ISAJET cross sections over various kinematic intervals.

Reconstruction of π^0's/Strip chamber

The minimum laboratory angle between photon pairs produced through the electromagnetic decay of mesons is given by

$$\Delta\theta_{min} = 2\frac{m}{E}, \tag{24}$$

where m is the mass and E is the laboratory energy of the decaying meson. For meson momenta P_m in the range $10 \leq P_m \leq 20$ GeV/c, $\Delta\theta_{min}$ varies from about 14 mr to 27 mr for π^0 decay. Expressed in terms of transverse momentum, $10 \leq P_T \leq 20$ GeV/c and $|\eta| \leq 1$ corresponds to $10 \leq P_m \leq 31$ GeV/c and to $9 \leq \Delta\theta_{min} \leq 27$ mr. Figure 9 shows the distribution of radial energy deposited in polystyrene scintillator by 10 GeV photon showers as calculated by the EGS computer program. With very fine segmentation and large distances, the two photons from π^0 decay can be distinguished from a single, isolated direct-γ event. However, the cost increases with finer segmentation or with increasing distance to the photon detector. Furthermore, highly asymmetric decays of mesons may cause the loss of one photon from the detector acceptance or may lead to the inability to identify the low-energy photon because of detector noise. Thus, realistic detectors cannot always disinguish true direct-γ events from electromagnetic decays of mesons.

The definition of the spin-spin correlation parameter A_{LL} for inclusive direct-γ production is

$$A_{LL} = \frac{1}{P_B^2} \cdot \frac{N_\gamma^+ - N_\gamma^-}{N_\gamma^+ + N_\gamma^-} \tag{25}$$

where $N_\gamma^\pm$ are the total number of direct-γ events, normalized to the beam luminosity, for beam spins parallel (+) and antiparallel (−). Note $|P_B^2 A_{LL}| \leq 1$ from the formula above, and $|A_{LL}| \leq 1$ for the physics parameter. Since $N_\gamma^\pm$ is not measured directly, it must be estimated from the total counts $n_{tot}^\pm$ (total

direct γ's + total unresolved "fake" γ's) and from the total number $n^{\pm}_{\pi^0}$ of reconstructed π^0's, η^0's, etc., using

$$N^{\pm}_{\gamma} = n^{\pm}_{tot} - R_{fake} \cdot n^{\pm}_{\pi^0}. \tag{26}$$

The symbol R_{fake} in Eq. 26 represents the ratio of the total number of γ's from unresolved π^0, η^0, etc. decays to the number of resolved π^0, η^0, etc. decays. Substitution of Eq. 26 into Eq. 25 yields the following relation:

$$A = A_{LL} = \frac{1}{P_B^2} \cdot \frac{n^{+}_{tot} - n^{-}_{tot} - R_{fake}\left(n^{+}_{\pi^0} - n^{-}_{\pi^0}\right)}{n^{+}_{tot} + n^{-}_{tot} - R_{fake}\left(n^{+}_{\pi^0} + n^{-}_{\pi^0}\right)}, \tag{27}$$

and its error, δA_{LL}:

$$\delta A_{LL} = \frac{1}{P_B^2} \cdot \frac{1}{\sqrt{N_\gamma}} \cdot \left[\left[1-(P_B^2 A)^2\right] + R_{fake} \cdot \frac{N_{\pi^0}}{N_\gamma} \cdot \left[1 + (P_B^2 A)^2 - 2(P_B^2 A)(P_B^2 B)\right]\right]^{\frac{1}{2}}. \tag{28}$$

In the previous expression, $A = A_{LL}$ for inclusive direct-γ production and B is the (background) asymmetry in inclusive π^0, η^0, etc. production. The quantities N_{π^0} and N_γ are estimated from Eqs. 20 and 18, respectively ($N_{\pi^0}/N_\gamma \simeq \sigma_{\pi^0}/\sigma_\gamma$).

For comparison with Eq. 22, the maximal value of δA_{LL} in Eq. 28 is given when the sign of B is opposite to the sign of A and $|B| = 1$. In terms of the parameter

$$\Gamma = R_{fake} \cdot N_{\pi^0}/N_\gamma, \tag{29}$$

the value of A_{LL} that maximizes Eq. 28 is

$$A = A_{LL} = \Gamma/(1-\Gamma). \tag{30}$$

For $\Gamma \geq 0.5$ we required $A = 1$, which leads to the two conditions:

$$\begin{aligned} \delta A_{LL} &\leq \frac{1}{P_B^2} \cdot \frac{1}{\sqrt{N_\gamma}} \cdot \left[1 + \Gamma + \frac{\Gamma^2}{(1-\Gamma)} \cdot P_B^4\right]^{\frac{1}{2}} \text{ for } \Gamma \leq \frac{1}{2}, \\ &\leq \frac{1}{P_B^2} \cdot \frac{1}{\sqrt{N_\gamma}} \cdot \left[1 + \Gamma + (3\Gamma - 1) \cdot P_B^4\right]^{\frac{1}{2}} \text{ for } \Gamma \geq \frac{1}{2}. \end{aligned} \tag{31}$$

Figure 10 is a plot of the "error factor" $Q = P_B^2 \cdot \sqrt{N_\gamma} \cdot \delta A_{LL}$ for $P_B = 0$ and 0.7 as a function of Γ.

The PHENIX photon detector is expected to consist of many crystal and lead glass elements of cross sectional area $\sim 5 \times 5$ cm^2 at a distance from the

interaction point of 5 m. This detector is to be located near $\theta_{lab} = 90°$ ($\eta = 0$) and will cover an area of $\Delta\eta \simeq 0.70$ and $\Delta\phi = 180°$ in two asymmetric arms with $\Delta\phi = 90°$ each. A simple Monte Carlo computer program was written to compute R_{fake} as a function of P_T for this detector, and the results are presented in Fig. 11. This result was obtained by considering only the loss of photons outside the detector acceptance, and thus represents a lower limit to R_{fake}. A sizeable fraction of the "fake" γ's originated from η^0 decays. Assuming $R_{fake} \simeq 0.035$ in Eq. 31, and taking into account the detector acceptance, the anticipated uncertainty on A_{LL} for a one month run at $\sqrt{s} = 200$ GeV at the design luminosity is

$$\delta A_{LL} \sim \frac{1}{P_B^2}(0.022/\sqrt{\text{month}}). \tag{32}$$

The STAR electromagnetic calorimeter design has "towers" with cross sectional area 13.3×13.6 cm^2 near $\theta_{min} = 90°$ and larger in one dimension at more forward angles. The calorimeter covers $-1.05 \leq \eta \leq 1.05$ and $\Delta\phi = 2\pi$. The inner radius is expected to be about 2.53 m, which gives a lower limit to the angular resolution of two showers of 53 mr. This is not sufficient for resolving π^0 decays with $10 \leq P_T \leq 20$ GeV/c. Algorithms, such as analysis of moments for energy deposited, will probably not improve the resolution by more than a factor of 2. Since the tower size is so large and the corresponding angular resolution so poor compared to the required values of $9-27$ mr, the electromagnetic calorimeter alone will not be useful for direct-γ measurements (R_{fake} will be too large to give meaningful results).

The spatial resolution for showers in the STAR calorimeter could be improved dramatically using a detector made of strips placed at a depth corresponding to the shower maximum in the calorimeter. Simulations were performed using 0.5, 1, or 1.5 cm wide strips of length corresponding to twice the tower dimension in η (28 - 45 cm) at a radius $R = 260$ cm. In the simulations, it was assumed that the photons could be resolved if $R\Delta\phi \geq 1$, 2, or 3 cm. The results of this conservative calculation are displayed in Fig. 12. With the 1 cm strips, the estimated δA_{LL} is

$$\delta A_{LL} \sim \frac{1}{P_B^2}(0.013/\sqrt{\text{month}}). \tag{33}$$

The error is increased by a factor of 1.2 for 1.5 cm strips, and is reduced by a factor of 1.3 for 0.5 cm strips. At $P_T \sim 20$ GeV/c we note $R\Delta\theta_{min} = 3.5$ cm, suggesting that the 1 cm width may be near optimum when cost vs. π° resolution is considered.

Preshower detector

In the discussion for this section, assume a detector configuration as shown in Fig. 13. From the interaction point, the particles first pass through an anticoin-

cidence counter for rejecting charged particles, then a preconvertor of thickness t radiation lengths, followed by a preshower detector and finally an EM calorimeter. As in the last section, it is assumed that the EM calorimeter cannot resolve fake photons.

The nonconversion probability[60] for single photons passing through the preconvertor is

$$\nu_\gamma = \exp\left[-\frac{7}{9}t(1-\xi)\right] \tag{34}$$

with the thickness of the preconvertor t expressed in units of radiation lengths (X_0), and with ξ being a small energy-dependent correction term. The nonconversion probability for two photons passing through the preconvertor at the same time (i.e. $\pi^0 \to \gamma\gamma$) is to good approximation the square of ν_γ, or $\nu_E = \nu_\gamma^2$.

The preshower scheme uses a statistical approach to establish a direct-γ signal. The N_{tot} photons detected in the EM calorimeter consist of N_{π^0} fake photons and N_γ direct photons, or

$$N_{tot}^{\pm} = N_{\pi^0}^{\pm} + N_\gamma^{\pm}, \tag{35}$$

where $+$, and $-$ correspond to parallel and antiparallel beam spins, respectively. The number of nonconverted photons (not tagged by the preshower detector) is just

$$N_{nc}^{\pm} = \nu_E N_{\pi^0}^{\pm} + \nu_\gamma N_\gamma^{\pm} = \nu_{nc}^{\pm} N_{tot}^{\pm}. \tag{36}$$

Since the measured quantities are only $N_{nc}^{\pm}$ and $N_{tot}^{\pm}$, the number of direct-γ's is estimated by

$$N_\gamma^{\pm} = \frac{\nu_{nc}^{\pm} - \nu_E}{\nu_\gamma - \nu_E} N_{tot}^{\pm}. \tag{37}$$

Inserting this into Eq. 25 leads to

$$A_{LL} = \frac{1}{P_B^2} \cdot \frac{(\nu_{nc}^{+} - \nu_E)N_{tot}^{+} - (\nu_{nc}^{-} - \nu_E)N_{tot}^{-}}{(\nu_{nc}^{+} - \nu_E)N_{tot}^{+} + (\nu_{nc}^{-} - \nu_E)N_{tot}^{-}}. \tag{38}$$

The two quantities N_{tot} and ν_{nc} are independent and have different types of errors – the former is governed by Poisson statistics, while the latter is governed by the binomial distribution. The error in A_{LL} is then

$$\delta A_{LL} = \frac{1}{P_B^2} \cdot \frac{1}{\sqrt{N_\gamma}} \cdot \frac{1}{\nu_\gamma - \nu_E} \cdot \Bigg[\left(\nu_E^2 + \nu_\gamma(1-2\nu_E)\right)\left[1-(P_B^2 A)^2\right] + \frac{N_{\pi^0}}{N_\gamma} \cdot \nu_E(1-\nu_E)\left[1+(P_B^2 A)^2 - 2(P_B^2 A)(P_B^2 B)\right] \Bigg]^{\frac{1}{2}}, \tag{39}$$

where again, $P_B^2 B$ is the background asymmetry and $A = A_{LL}$.

For large values of P_B, there is a physically allowable value of A that maximizes δA_{LL} in Eq. 39. It can be shown that the condition $0 \leq A \leq 1$ is equivalent to

$$1 + \nu_\gamma - \nu_\gamma^2 \geq 2\frac{N_{\pi^0}}{N_\gamma}\nu_\gamma(1+\nu_\gamma) \tag{40}$$

or

$$\nu_\gamma \leq \nu_{critical} \equiv \frac{1}{2}\left[\sqrt{1+\frac{4}{(2\frac{N_{\pi^0}}{N_\gamma}+1)^2}}-1\right] + \frac{1}{(2\frac{N_{\pi^0}}{N_\gamma}+1)^2}. \tag{41}$$

The value of $A = A_{LL}$ can be substituted into Eq. 39 and the resulting expression minimized as a function of ν_γ, assuming $\nu_E = \nu_\gamma^2$. The minimization leads to solving a sixth order polynomial in ν_γ.

As in the last section, the value of δA_{LL} is maximized for most values of P_B when $A = \pm 1$ and $B = -A$:

$$\delta A_{LL} \leq \frac{1}{P_B^2}\cdot\frac{1}{\sqrt{N_\gamma}}\cdot\frac{1}{\nu_\gamma-\nu_E}\cdot\left[\left(\nu_E^2+\nu_\gamma(1-2\nu_E)\right)\left[1-P_B^4\right] + \frac{N_{\pi^0}}{N_\gamma}\cdot\nu_E(1-\nu_E)\cdot\left[1+3P_B^4\right]\right]^{\frac{1}{2}}. \tag{42}$$

Figure 14 is a plot of $P_B^2\sqrt{N_\gamma}\delta A_{LL}$, with δA_{LL} given by Eq. 42, as a function of the nonconversion probability ν_γ for two values of P_B. In general, the error can be minimized as a function of P_B by adjusting the thickness of the preconvertor. With the approximation that $\nu_E \simeq \nu_\gamma^2$, then the desired relation is:

$$\nu_\gamma \simeq \frac{\sqrt{1+X}-1}{X}, \qquad X = \frac{2N_{\pi^0}}{N_\gamma}\frac{1+3P_B^4}{1-P_B^4}. \tag{43}$$

Using the estimated cross section ratio, then $N_{\pi^0}/N_\gamma \simeq 6$. Figure 15 gives a plot of the optimum absorber thickness t from Eq. 34 that minimizes the error in Eq. 42 as a function of the beam polarization P_B. It can be seen that the ideal preconvertor thickness corresponds to roughly two radiation lengths ($2X_0$). As noted above, the relations in Eq. 43 do not apply for $\nu \leq \nu_{critical} = 0.0828$, or $t \geq t_{critical} = 3.20X_0$, or $P_B \geq P_{B,critical} = 0.913$ with $N_{\pi^0}/N_\gamma \simeq 6$. (For $N_{\pi^0}/N_\gamma \simeq 5$, the corresponding values are $\nu_{critical} = 0.0991$, $t_{critical} = 2.97X_0$, and $P_{B,critical} = 0.895$.)

Inserting this ν_γ into Eq. 42 and using the estimated cross section ratio yields an uncertainty,

$$\begin{aligned} \delta A_{LL} &\leq \frac{1}{P_B^2\sqrt{N_\gamma}}\sqrt{\frac{(1-P_B^4)}{2}[4\sqrt{X+1}+X+6]} \\ &\simeq \frac{1}{P_B^2}(0.036/\sqrt{\text{month}}). \end{aligned} \tag{44}$$

This value of δA_{LL} is also plotted in Fig. 15. A comparison of this result with those of Eqs. 32 and 33 show the preconvertor to be worse than using either π°-reconstruction for PHENIX or a strip chamber in STAR. On the other hand, at high enough P_T, the preconvertor method will continue to work whereas the shower separations from $\pi^0 \to \gamma\gamma$ decays become smaller than the radius of a shower and thus too small to separate.

Kinematics and Rates for Inclusive Direct-γ + Jet Production

In order to measure $G(x)$, both the direct-γ and the "away-side" jet must be detected in coincidence so that the kinematics of the incoming partons can be calculated. In this section, these kinematics will be discussed first, followed by calculation of rates and of δA_{LL} in various kinematic regions. Details of the jet detection will not be included, except to require acceptance about the jet direction corresponding to $\sqrt{(\Delta\eta)^2+(\Delta\phi)^2} = 0.7$. Thus, a central barrel calorimeter extending to $|\eta| \leq 1.0$ will be assumed to permit jet detection only for $|\eta_{Jet}| \leq 0.3$, and a combined barrel and endcap calorimeter with $|\eta| \leq 2.0$ would allow jets to $|\eta_{Jet}| \leq 1.3$.

The Compton and annihilation subprocesses both involve $2 \to 2$ scatterings, shown schematically in the laboratory frame in Fig. 16. The incoming partons are assumed to have fractions x_1 and x_2 of the beam momentum, and to have negligible transverse momentum, so that they collide collinearly. The outgoing partons are at angles θ_1 and θ_2 relative to the incoming direction of parton 1. Conservation of momentum transverse to the beam gives

$$P_T = P_1 \sin\theta_1 = P_2 \sin\theta_2, \tag{45}$$

and along the beam gives

$$\begin{aligned} x_1 - x_2 &= (P_1\cos\theta_1 + P_2\cos\theta_2)/P_L \\ &\simeq \frac{2P_T}{\sqrt{s}}(\frac{\cos\theta_1}{\sin\theta_1} + \frac{\cos\theta_2}{\sin\theta_2}). \end{aligned} \tag{46}$$

Expressed in terms of pseudorapidity,

$$\eta = -\log(\tan(\theta/2)), \tag{47}$$

then

$$x_1 - x_2 \simeq \frac{2P_T}{\sqrt{s}}(\sinh\eta_1 + \sinh\eta_2). \tag{48}$$

Evaluating the total energy $\hat{s}$ at the parton level for the incoming and outgoing states, and ignoring quark masses, leads to

$$\begin{aligned} x_1 + x_2 &\simeq \frac{2P_T}{\sqrt{s}}(\frac{1}{\sin\theta_1} + \frac{1}{\sin\theta_2}) \\ &\simeq \frac{2P_T}{\sqrt{s}}(\cosh\eta_1 + \cosh\eta_2). \end{aligned} \tag{49}$$

Finally, combining Eqs. 48 and 49 gives

$$\begin{aligned} x_1 &\simeq \frac{2P_T}{\sqrt{s}}(\frac{e^{\eta_1} + e^{\eta_2}}{2}) \\ x_2 &\simeq \frac{2P_T}{\sqrt{s}}(\frac{e^{-\eta_1} + e^{-\eta_2}}{2}). \end{aligned} \tag{50}$$

In a Monte Carlo one assumes complete factorization and one can also trace from a final observable particle to an initial parton. Since in real data there can be an ambiquity in identifying the inital partons, we describe our results in terms of the larger reconstructed x, x_b, and the smaller one, x_a. By placing limits on one x, we enhance the probability that at least one parton is a quark with large polarization. It was concluded in the Physics Motivation section that in order to measure $\Delta G(x)$, the x of the quark must be larger than 0.2 to 0.3 so that $|\Delta q(x)|$ would be sizeable. Figure 17 shows the range of x (x_a) that could be measured in an experiment with $|\eta_\gamma| < 1.0$ and $|\eta_{jet}| < 0.3$ as a function of $\sqrt{s}$. The second x (x_b) is required to be greater than 0.2, and the events would have $P_T = 10$ or 20 GeV/c. For both P_T values, the range of x is very limited except at low $\sqrt{s}$, where the cross section and luminosity are small. Figure 18 presents similar plots for $|\eta_\gamma| < 2.0$ and $|\eta_{Jet}| < 1.3$, and x_b larger than $0.2, 0.25$, and 0.3. In this case, there is a reasonable range available for $P_T = 10$ GeV/c and $x_b > 0.2$ below $\sqrt{s} \sim 350$ GeV, or for $x_b > 0.3$ and the same P_T below $\sqrt{s} \sim 250$ GeV. A very broad x_a range is available with $P_T = 20$ GeV/c, but the rates are much lower.

Another way of presenting these data is shown in Fig. 19. Curves of constant x_1 and x_2 are shown for $\sqrt{s} = 200$ GeV and $P_T = 10$ GeV/c. From this information, regions of η_γ and η_{Jet} corresponding to $x_b > 0.2$ can be found. These are displayed as the shaded regions in Fig. 20. It is clear that an endcap calorimeter is needed under these circumstances. There is essentially no shaded area within the acceptance of the barrel calorimeter ($|\eta_\gamma| < 1.0$ and $|\eta_{Jet}| < 0.3$), shown as the inner rectangle. This conclusion is consistent with the conclusions of Fig. 17.

In order to determine an optimum $\sqrt{s}$ to perform the inclusive direct-γ + jet production spin measurements, detailed estimates of rates and δA_{LL} are required. ISAJET was used to generate $\mathcal{N}_{tot}$ "PHOTON" events for $|\eta_\gamma| \leq 2$, $|\eta_{jet}| \leq 1.3$, and $10 \leq P_T \leq 20$ GeV/c. Of these $\mathcal{N}_{tot}$ events, n_a had $x_b \geq 0.2$. The total n_a at each $\sqrt{s}$ was scaled to 1-RHIC-month using the equivalent integral luminosity for the simulation at that $\sqrt{s}$ and the integral design luminosity for RHIC (Table 6 and Fig. 7):

$$\int_{RHIC} Ldt = \frac{0.7252 \text{ E+08}}{\text{mb–GeV}} \cdot \sqrt{s}. \tag{51}$$

Table 8 and Fig. 21 summarize the results. We note that while the cross section increases with $\sqrt{s}$, the fraction of γ+jet events with $x_b \geq 0.2$ falls off exponentially, resulting in a n_a plateau starting near 200 GeV. The x_a distribution (dn_a/dx_a) at $\sqrt{s} = 200$ GeV is shown in Fig. 22. The width of the distribution is 0.044 and its mean is 0.078. The most probable x_a is 0.048.

The ISAJET simulation at $\sqrt{s} = 200$ GeV was used to estimate δA_{LL} for various Δx_a, Δx_b regions. For each event, x_1 and x_2 were calculated and the smaller taken as x_a (i.e., gluon), and the larger taken as x_b (i.e., quark). Table 9 shows δA_{LL} for $P_T \geq 10$ GeV/c, scaled to 1-RHIC-month for both design and enhanced luminosities. The polarization was assumed $P_B = 0.7$.

Conclusions

A number of different schemes were considered for measurements of spin effects in inclusive direct-γ production. The errors that were derived can be parameterized as

$$\delta A_{LL} = \frac{1}{P_B^2} \cdot \frac{1}{\sqrt{N_\gamma}} \cdot \mathcal{Q}_{max}. \tag{52}$$

Table 10 lists the various forms of $\mathcal{Q}_{max}$ (maximal error factor) for the different direct-γ detection schemes discussed. For the preshower/preconvertor $\nu_E \sim \nu_\gamma^2$ has been used in Eq. 42 to simplify the final form shown in Table 10.

The different schemes to measure inclusive direct-γ production can be compared for the "standard conditions," $\sqrt{s} = 200$ GeV, $10 \leq P_T \leq 20$ GeV/c, beam polarizations $P_B = 0.7$, the design luminosity $L = 5.6 \times 10^{30}/\text{cm}^2/\text{sec}$ and a one month run with 100% operating efficiency. The estimated errors δA_{LL} were: $\delta A_{LL} \leq \pm 0.016$ for an ideal detector with $\Delta\eta = 2$ and $\Delta\phi = 2\pi$, $\delta A_{LL} \leq \pm 0.045$ for the PHENIX detector with fine segmentation, $\delta A_{LL} \leq \pm 0.027$ for the STAR detector with a strip chamber or strips of scintillator of 1 cm width at shower maximum depth in the electromagnetic calorimeter, and $\delta A_{LL} \leq \pm 0.074$ for a preshower detector with a preconvertor thickness of roughly $2X_0$ and $\Delta\eta = 2$, $\Delta\phi = 2\pi$. Thus, STAR with a shower maximum

detector of 1 cm wide strips and PHENIX with fine segmentation are expected to give roughly equal errors, which will be about twice that for an ideal detector. Although a preshower detector might be essential at higher P_T, it does not seem as useful for the measurements described here ($10 \leq P_T \leq 20$ GeV/c).

For measurements of $\Delta G(x)$, both the direct-γ and the away-side jet must be detected in coincidence. The kinematics to have one x large enough to give a sizeable quark polarization require an end cap calorimeter in addition to the barrel electromagnetic calorimeter. It appears that the optimum energy for these measurements will be near $\sqrt{s} \sim 200$ GeV, in order to get sufficient rate and range of x for the gluon. In this case, to obtain sufficient numbers of inclusive direct-γ + jet events may require runs with high luminosity in RHIC.

These error estimates also suggest that a number of months running time will be needed at the design luminosity to distinguish differences of order $\delta A_{LL} \sim 0.05$ between various theoretical estimates of ΔG. Runs with high luminosity in RHIC will produce a substantial reduction in δA_{LL} for a given running time.

Acknowledgements

We wish to thank E. Berger, G. Bodwin, and G. Ramsey for useful theoretical discussions; D. Grosnick and D. Lopiano for a careful reading of the paper; and D. Lopiano for assistance with some of the figures and calculations.

References

[1] M. J. Alguard, W. W. Ash, G. Baum, J. E. Clendenin, P. S. Cooper, D. H. Coward, R. D. Ehrlich, A. Etkin, V. W. Hughes, H. Kobayakawa, K. Kondo, M. S. Lubell, R. H. Miller, D. A. Palmer, W. Raith, N. Sasao, K. P. Schüler, D. J. Sherden, C. K. Sinclair, and P. A. Souder, Phys. Rev. Lett. **37**, 1261 (1976).

[2] M. J. Alguard, W. W. Ash, G. Baum, M. R. Bergstrom, J. E. Clendenin, P. S. Cooper, D. H. Coward, R. D. Ehrlich, V. W. Hughes, K. Kondo, M. S. Lubell, R. H. Miller, S. Miyashita, D. A. Palmer, W. Raith, N. Sasao, K. P. Schüler, D. J. Sherden, P. A. Souder, and M. E. Zeller, Phys. Rev. Lett. **41**, 70 (1978).

[3] V. W. Hughes and J. Kuti, Ann. Rev. Nucl. Part. Sci. **33**, 611 (1983).

[4] J. Ashman, B. Badelek, G. Baum, J. Beaufays, C. P. Bee, C. Benchouk, I. G. Bird, S. C. Brown, M. C. Caputo, H. W. K. Cheung, J. Chima, J. Ciborowski, R. W. Clifft, G. Coignet, F. Combley, G. Court, G. D'Agostini, J. Drees, M. Düren, N. Dyce, A. W. Edwards, M. Edwards, T. Ernst, M. I. Ferrero, D. Francis, E. Gabathuler, J. Gajewski, R. Gamet, V. Gibson, J. Gillies, P. Grafström, K. Hamacher, D. von Harrach, P. Hayman, J. R. Holt, V. W. Hughes, A. Jacholkowska, T. Jones, E. M. Kabuss, B. Korzen, U. Krüner, S. Kullander, U. Landgraf, D. Lanske, F. Lettenström, T. Lindqvist, J. Loken, M. Matthews, Y. Mizuno, K. Mönig, F. Montanet, J. Nassalski, T. Niinikoski, P. R. Norton, G. Oakham, R. F. Oppenheim, A. M. Osborne, V. Papavassiliou, N. Pavel, C. Peroni, H. Peschel, R. Piegaia, B. Pietrzyk, U. Pietrzyk, B. Povh, P. Renton, J. M. Rieubland, A. Rijllart, K. Rith, E. Rondio, L. Ropelewski, D. Salmon, A. Sandacz, T. Schröder, K. P. Schüler, K. Schultze, T.-A. Shibata, T. Sloan, A. Staiano, H. Stier, J. Stock, G. N. Taylor, J. C. Thompson, T. Walcher, S. Wheeler, W. S. C. Williams, S. J. Wimpenny, R. Windmolders, W. J. Womersley, and K. Ziemons, Phys. Lett. **206B**, 364 (1988).

[5] V. W. Hughes, V. Papavassiliou, R. Piegaia, K. P. Schuler, and G. Baum, Phys. Lett. **212B**, 511 (1988).

[6] A. V. Efremov, American Institute of Physics Proceedings **223**, 80 (1991); A. V. Manohar, ibid., 90 (1991); R. D. Carlitz and R. S. Willey, ibid., 1991 (1991).

[7] F. E. Close and D. Sivers, Phys. Rev. Lett. **39**, 1116 (1977).

[8] J. P. Ralston and D. E. Soper, Nucl. Phys. **B152**, 109 (1979).

[9] K. Hidaka, Phys. Rev. **D21**, 1316 (1980).

[10] H. S. Mani and M. Noman, Phys. Rev. **D24**, 1223 (1981).

[11] B. Pire and J. P. Ralston, Phys. Rev. **D28**, 260 (1983).

[12] R. D. Carlitz and R. S. Willey, Phys. Rev. **D45**, 2323 (1992).

[13] N. S. Craigie, K. Hidaka, M. Jacob, and F. M. Renard, Phys. Rep. **99C**, 69 (1983).

[14] M. B. Einhorn and J. Soffer, Nucl. Phys. **B274**, 714 (1986).

[15] E. L. Berger and J. Qiu, Phys. Rev. **D40**, 778 (1989); 3128 (1989); American Institute of Physics Conference Proceedings **223**, 162 (1991).

[16] P. Mathews and R. Ramachandran, Z. Phys. **C53**, 305 (1992).

[17] M. Glück and W. Vogelsang, Phys. Lett. **277B**, 515 (1992).

[18] J. Babcock, E. Monsay, and D. Sivers, Phys. Rev. **D19**, 1483 (1979).

[19] P. Chiappetta and G. Nardulli, Z. Phys. **C51**, 435 (1991).

[20] J. Ph. Guillet, American Institute of Physics Conference Proceedings **223**, 155 (1991).

[21] J. F. Owens, Rev. Mod. Phys. **59**, 465 (1987).

[22] T. Ferbel and W. R. Molzon, Rev. Mod. Phys. **56**, 181 (1984).

[23] E. L. Berger, E. Braaten, and R. D. Field, Nucl. Phys. **B239**, 52 (1984).

[24] T. Åkesson, M. G. Albrow, S. Almehed, E. Anassontzis, R. Batley, O. Benary, H. Bøggild, O. Botner, H. Breuker, V. Burkert, B. Callen, R. Carosi, A. A. Carter, J. R. Carter, P. C. Cecil, V. Chernyatin, Y. Choi, W. E. Cleland, S. Dagan, E. Dahl-Jensen, I. Dahl-Jensen, P. Dam, G. Damgaard, B. Dolgoshein, S. Eidelman, M. W. Evans, C. W. Fabjan, I. Gavrilenko, U. Goerlach, Y. Goloubkov, H. Gordon, K. H. Hansen, V. Hedberg, J. W. Hiddleston, P. Ioannou, G. Jarlskog, T. Jensen, A. Kalinovsky, V. Kantserov, S. Katsanevas, C. Kourkoumelis, R. Kroeger, K. Kulka, D. Lissauer, B. Lörstad, I. Mannelli, A. Markou, S. Mayburov, N. A. McCubbin, U. Mjörnmark, R. Møller, W. Molzon, P. Nevsky, B. S. Nielsen, L. H. Olsen, Y. Oren, G. Piskounov, D. C. Rahm, L. K. Resvanis, A. Rudge, J. Schukraft, A. Shmeleva, V. Sidorov, S. Smirnov, H. Specht, N. Starinsky, I. Stumer, M. Sullivan, H. H. Thodberg, J. A. Thompson, G. Thorstenson, A. Vanjashin, E. Vella, J. Williamson, W. J. Willis, M. Winik, and C. Woody, Z. Phys. **C34**, 293 (1987). (ISR - AFS Collaboration)

[25] L. Cormell and J. F. Owens, Phys. Rev. **D22**, 1609 (1980).

[26] F. Halzen, M. Dechantsreiter, and D. M. Scott, Phys. Rev. **D22**, 1617 (1980).

[27] R. Baier, J. Engels, and B. Petersson, Z. Phys. **C6**, 309 (1980).

[28] A. P. Cantogouris, S. Papadopoulos, and C. Papavassiliou, Nucl. Phys. **B179**, 461 (1981).

[29] R. R. Horgan and P. N. Scharbach, Nucl. Phys. **B181**, 421 (1981).

[30] For example, see J. G. Morfin and W. K. Tung, Z. Phys. **C52**, 13 (1991).

[31] P. Aurenche, A. Douiri, R. Baier, M. Fontannaz, and D. Schiff, Phys. Lett. **140B**, 87 (1984).

[32] E. L. Berger and J. Qiu, Phys. Rev. **D44**, 2002 (1991).

[33] G. Altarelli and G. G. Ross, Phys. Lett. **212B**, 391 (1988).

[34] R. D. Carlitz, J. C. Collins, and A. H. Mueller, Phys. Lett. **214B**, 229 (1988).

[35] J. D. Bjorken, Phys. Rev. **148**, 1467 (1966); **D1**, 1376 (1970).

[36] For example, see M. Bourquin, R. M. Brown, Y. Chatelus, J. C. Chollet, A. Degré, D. Froidevaux, A. R. Fyfe, J. -M. Gaillard, C. N. P. Gee, W. M. Gibson, R. J. Gray, P. Igo-Kemenes, P. W. Jeffreys, B. Merkel, R. Murand, R. J. Ott, H. Plothow, J. -P. Repellin, B. J. Saunders, G. Sauvage, B. Schiby, H. W. Siebert, V. J. Smith, K. P. Streit, R. Strub, and J. J. Thresher, Z. Phys. **C21**, 27 (1983).

[37] G. T. Bodwin and J. Qiu, Phys. Rev. **D41**, 2755 (1990).

[38] C. De Marzo, M. De Palma, C. Favuzzi, G. Maggi, E. Nappi, F. Posa, A. Ranieri, G. Selvaggi, P. Spinelli, A. Bamberger, M. Fuchs, W. Heck, C. Loos, R. Marx, K. Runge, E. Skodzek, C. Weber, M. Wülker, F. Zetsche, V. Artemiev, Yu. Galaktionov, A. Gordeev, Yu. Gorodkov, Yu. Kamyshkov, V. Plyaskin, V. Pojidaev, V. Shevchenko, E. Shumilov, V. Tchudakov, J. Bunn, J. Fent, P. Freund, J. Gebauer, M. Glas, P. Polakos, K. Pretzl, T. Schouten, P. Seyboth, J. Seyerlein, and G. Vesztergombi, Phys. Rev. **D36**, 8 (1987). (NA24 Collaboration)

[39] M. Bonesini, E. Bonvin, P. S. L. Booth, L. J. Carroll, A. J. Cass, D. Cavalli, G. Cecchet, G. Costa, M. Donnat, P. A. Dorsaz, D. N. Edwards, J. R. Fischer, L. Fluri, D. Frame, F. Gianotti, S. Jack, J. N. Jackson, M. Kelly, M. N. Kienzle-Focacci, R. Lucock, J. G. Lynch, L. Mandelli, M. Martin, L. Mathys, A. Maxwell, M. Mazzanti, J. J. Myerscough, P. J. Negus, S. Pensotti-Rancoita, L. Perini, D. Perrin, G. Polesello, W. H. Range, L. Rosselet, S. W. Snow, A. S. Thompson, R. M. Turnbull, J. Wells, and M. Werlen, Z. Phys. **C38**, 371 (1988). (WA70 Collaboration)

[40] A. Bernasconi, R. E. Breedon, L. Camilleri, R. L. Cool, P. T. Cox, L. Dick, E. C. Dukes, B. Gabioud, F. Gaille, P. Giacomelli, J. B. Jeanneret, C. Joseph, W. Kubischta, J. F. Loude, E. Malamud, C. Morel, O. E. Overseth, J. L. Pagès, J. P. Perroud, P. Petersen, D. Ruegger, R. W. Rusack, G. R. Snow, G. Sozzi, M.-T. Tran, A. Vacchi, G. Valenti, and G. von Dardel, Phys. Lett. **206B**, 163 (1988). (UA6 Collaboration)

[41] A. L. S. Angelis, H.-J. Besch, B. J. Blumenfeld, L. Camilleri, T. J. Chapin, R. L. Cool, C. del Papa, L. Di Lella, Z. Dimčovski, R. J. Hollebeek, L. M. Lederman, D. A. Levinthal, J. T. Linnemann, C. B. Newman, N. Phinney, B. G. Pope, S. H. Pordes, A. F. Rothenberg, R. W. Rusack, A. M. Segar, J. Singh-Sidhu, A. M. Smith, M. J. Tannenbaum, R. A. Vidal, J. S. Wallace-Hadrill, J. M. Yelton, and K. K. Young, Phys. Lett. **94B**, 106 (1980). (CCOR - R110 Collaboration)

[42] E. Anassontzis, A. Karabarbounis, C. Kourkoumelis, L. K. Resvanis, R. B. Palmer, D. C. Rahm, P. Rehak, I. Stumer, C. W. Fabjan, T. Ferbel, D. Lissauer, I. Mannelli, W. Molzon, P. Mouzourakis, A. Nappi, E. Rosso, and W. Willis, Z. Phys. **C13**, 277 (1982). (ISR - R806 Collaboration)

[43] R. Ansari, P. Bagnaia, M. Banner, R. Battiston, K. Bernlöhr, C. Booth, K. Borer, M. Borghini, G. Carboni, V. Cavasinni, P. Cenci, J.-C. Chollet, A. G. Clark, C. Conta, C. Corona, F. Costantini, P. Darriulat, B. De Lotto, T. Del Prete, L. Di Lella, J. Dines Hansen, K. Einsweiler, L. Fayard, R. Ferrari, M. Fraternali, D. Froidevaux, J.-M. Gaillard, O. Gildemeister, V. G. Goggi, C. Gössling, B. Hahn, H. Hänni, J. R. Hansen, P. Hansen, K. Hara, N. Harnew, H. Hugentobler, E. Iacopini, L. Iconomidou-Fayard, K. Jacobs, P. Jenni, E. E. Kluge, O. Kofoed-Hansen, S. Lami, E. Lançon, P. Lariccia, M. Livan, S. Loucatos, B. Madsen, B. Mansoulié, G. C. Mantovani, L. Mapelli, K. Meier, B. Merkel, R. Møllerud, M. Moniez, R. Moning, M. Morganti, C. Onions, T. Pal, M. A. Parker, G. Parrour, F. Pastore, M. Pepe, C. Petridou, H. Plothow-Besch, M. Polverel, L. Rasmussen, J.-P. Repellin, A. Roussarie, V. Ruhlmann, G. Sauvage, J. Schacher, S. Stapnes, F. Stocker, M. Swartz, J. Teiger, W. Y. Tsang, M. Valdata-Nappi, V. Vercesi, A. R. Weidberg, M. Wunsch, and H. Zaccone, Z. Phys. **C41**, 395 (1988); J. A. Appel, P. Bagnaia, M. Banner, R. Battiston, K. Bernlöhr, K. Borer, M. Borghini, G. Carboni, V. Cavasinni, P. Cenci, J. C. Chollet, A. G. Clark, C. Conta, P. Darriulat, B. De Lotto, T. Del Prete, L. D. Di Lella, J. Dines-Hansen, K. Einsweiler, R. Engelmann, L. Fayard, M. Fraternali, D. Froidevaux, J. M. Gaillard, O. Gildemeister, V. G. Goggi, C. Gössling, B. Hahn, H. Hänni, J. R. Hansen, P. Hansen, N. Harnew, T. Himel, L. Iconomidou-Fayard, K. Jacobs, P. Jenni, E. E. Kluge, O. Kofoed-Hansen, E. Lançon, M. Livan, S. Loucatos, B. Madsen, P. Mani, B. Mansoulié, G. C. Mantovani, L. Mapelli, K. Meier, B. Merkel, R. Mollerud, M. Moniez, R. Moning, M. Morganti, C. Onions, M. A. Parker, G. Parrour, F. Pas-

tore, M. Pepe, H. Plothow-Besch, M. Polverel, J.-P. Repellin, A. F. Rothenberg, A. Roussarie, V. Ruhlmann, G. Sauvage, J. Schacher, M. Schlötelburg, F. Stocker, M. Swartz, J. Teiger, S. N. Tovey, W. Y. Tsang, M. Valdata-Nappi, V. Vercesi, A. R. Weidberg, M. Wunsch, and H. Zaccone, Phys. Lett. **176B**, 239 (1986). (UA2 Collaboration)

[44] C. Albajar, M. G. Albrow, O. C. Allkofer, A. Astbury, B. Aubert, T. Axon, C. Bacci, T. Bacon, N. Bains, J. R. Batley, G. Bauer, S. Beingessner, A. Bettini, A. Bezaguet, R. Bonino, K. Bos, E. Buckley, G. Busetto, P. Catz, P. Cennini, S. Centro, F. Ceradini, D. G. Charlton, G. Ciapetti, S. Cittolin, D. Clarke, D. Cline, C. Cochet, J. Colas, P. Colas, M. Corden, J. A. Coughlan, G. Cox, D. Dau, J. P. Debrion, M. Degiorgi, M. Della Negra, M. Demoulin, D. Denegri, A. Diciaccio, F. J. Diez Hedo, L. Dobrzynski, J. Dorenbosch, J. D. Dowell, E. Duchovni, K. Eggert, E. Eisenhandler, N. Ellis, P. Erhard, H. Faissner, I. F. Fensome, A. Ferrando, M. Fincke-Keeler, P. Flynn, G. Fontaine, J. Garvey, D. Gee, S. Geer, A. Geiser, C. Ghesquiere, P. Ghez, C. Ghiglino, Y. Giraud-Heraud, A. Givernaud, A. Gonidec, H. Grassmann, J. M. Gregory, W. Haynes, S. J. Haywood, D. J. Holthuizen, M. Ikeda, W. Jank, M. Jimack, G. Jorat, D. Joyce, P. I. P. Kalmus, V. Karimäki, R. Keeler, I. Kenyon, A. Kernan, A. Khan, W. Kienzle, R. Kinnunen, M. Krammer, J. Kroll, D. Kryn, F. Lacava, M. Landon, J. P. Lees, R. Leuchs, S. Levegrün, S. Li, M. Lindgren, D. Linglin, P. Lipa, E. Locci, T. Markiewicz, C. Markou, M. Markytan, M. A. Marquina, G. Maurin, J.-P. Mendiburu, A. Meneguzzo, J. P. Merlo, T. Meyer, M.-N. Minard, M. Mohammadi, K. Morgan, H.-G. Moser, A. Moulin, B. Mours, Th. Muller, L. Naumann, P. Nedelec, A. Nisati, A. Norton, F. Pauss, C. Perault, E. Petrolo, G. Piano Mortari, E. Pietarinen, C. Pigot, M. Pimiä, A. Placci, J.-P. Porte, M. Preischl, E. Radermacher, T. Redelberger, H. Reithler, J.-P. Revol, D. Robinson, T. Rodrigo, J. Rohlf, C. Rubbia, G. Sajot, G. Salvini, J. Sass, D. Samyn, D. Schinzel, M. Schröder, A. Schwartz, W. Scott, C. Seez, T. P. Shah, I. Sheer, I. Siotis, D. Smith, R. Sobie, P. Sphicas, J. Strauss, J. Streets, C. Stubenrauch, D. Summers, K. Sumorok, F. Szoncso, C. Tao, A. Taurok, I. Ten Have, S. Tether, G. Thompson, E. Tscheslog, J. Tuominiemi, W. van de Guchte, A. van Dijk, B. van Eijk, J. P. Vialle, L. Villasenor, T. S. Virdee, W. von Schlippe, J. Vrana, V. Vuillemin, K. Wacker, G. Walzel, A. Wildish, I. Wingerter, S. J. Wimpenny, X. Wu, C.-E. Wulz, T. Wyatt, M. Yvert, C. Zaccardelli, I. Zacharov, N. Zaganidis, L. Zanello, and P. Zotto, Phys. Lett. **209B**, 385 (1988). (UA1 Collaboration)

[45] F. Abe, D. Amidei, G. Apollinari, M. Atac, P. Auchincloss, A. R. Baden, N. Bacchetta, M. W. Bailey, A. Bamberger, P. de Barbaro, B. A. Barnett, A. Barbaro-Galtieri, V. E. Barnes, T. Baumann, F. Bedeschi, S. Behrends, S. Belforte, G. Bellettini, J. Bellinger, D. Benjamin, J. Bensinger, A. Beretvas, J. P. Berge, S. Bertolucci, S. Bhadra, M. Binkley, D. Bisello, R. Blair, C. Blocker, A. Bodek, V. Bolognesi, A. W. Booth, C. Boswell,

G. Brandenburg, D. Brown, E. Buckley-Geer, H. S. Budd, G. Busetto, A. Byon-Wagner, K. L. Byrum, C. Campagnari, M. Campbell, A. Caner, R. Carey, W. Carithers, D. Carlsmith, J. T. Carroll, R. Cashmore, A. Castro, F. Cervelli, K. Chadwick, G. Chiarelli, W. Chinowsky, S. Cihangir, A. G. Clark, M. Cobal, D. Connor, M. Contreras, J. Cooper, M. Cordelli, D. Crane, M. Curatolo, C. Day, F. DeJongh, S. Dell'Agnello, M. Dell'Orso, L. Demortier, B. Denby, P. F. Derwent, T. Devlin, D. DiBitonto, M. Dickson, R. B. Drucker, K. Einsweiler, J. E. Elias, R. Ely, S. Eno, S. Errede, B. Esposito, A. Etchegoyen, B. Flaugher, G. W. Foster, M. Franklin, J. Freeman, H. Frisch, T. Fuess, Y. Fukui, A. F. Garfinkel, A. Gauthier, S. Geer, D. W. Gerdes, P. Giannetti, N. Giokaris, P. Giromini, L. Gladney, M. Gold, K. Goulianos, H. Grassmann, J. Grieco, C. Grosso-Pilcher, C. Haber, S. R. Hahn, R. Handler, K. Hara, B. Harral, R. M. Harris, J. Hauser, C. Hawk, T. Hessing, R. Hollebeek, L. Holloway, P. Hu, B. Hubbard, B. T. Huffman, R. Hughes, P. Hurst, J. Huth, J. Hylen, M. Incagli, T. Ino, H. Iso, H. Jensen, C. P. Jessop, R. P. Johnson, U. Joshi, R. W. Kadel, T. Kamon, S. Kanda, D. A. Kardelis, I. Karliner, E. Kearns, L. Keeble, R. Kephart, P. Kesten, R. M. Keup, H. Keutelian, D. Kim, S. Kim, L. Kirsch, K. Kondo, J. Konigsberg, E. Kovacs, S. E. Kuhlmann, E. Kuns, A. T. Laasanen, J. I. Lamoureux, S. Leone, J. Lewis, W. Li, P. Limon, T. M. Liss, N. Lockyer, M. Loreti, E. Low, C. B. Luchini, P. Lukens, P. Maas, K. Maeshima, M. Mangano, J. P. Marriner, M. Mariotti, R. Markeloff, L. A. Markosky, R. Mattingly, P. McIntyre, A. Menzione, T. Meyer, S. Mikamo, M. Miller, T. Mimashi, S. Miscetti, M. Mishina, S. Miyashita, Y. Morita, S. Moulding, J. Mueller, A. Mukherjee, L. F. Nakae, I. Nakano, C. Nelson, C. Newman-Holmes, J. S. T. Ng, M. Ninomiya, L. Nodulman, S. Ogawa, R. Paoletti, V. Papadimitriou, A. Para, E. Pare, S. Park, J. Patrick, G. Pauletta, L. Pescara, T. J. Phillips, F. Ptohos, R. Plunkett, L. Pondrom, J. Proudfoot, G. Punzi, D. Quarrie, K. Ragan, G. Redlinger, J. Rhoades, M. Roach, F. Rimondi, L. Ristori, T. Rodrigo, T. Rohaly, A. Roodman, W. K. Sakumoto, A. Sansoni, R. D. Sard, A. Savoy-Navarro, V. Scarpine, P. Schlabach, E. E. Schmidt, O. Schneider, M. H. Schub, R. Schwitters, A. Scribano, S. Segler, Y. Seiya, M. Shapiro, N. M. Shaw, M. Sheaff, M. Shochet, J. Siegrist, P. Sinervo, J. Skarha, K. Sliwa, D. A. Smith, F. D. Snider, L. Song, M. Spahn, P. Sphicas, R. St. Denis, A. Stefanini, G. Sullivan, R. L. Swartz, M. Takano, F. Tartarelli, K. Takikawa, S. Tarem, D. Theriot, M. Timko, P. Tipton, S. Tkaczyk, A. Tollestrup, J. Tonnison, W. Trischuk, N. Turini, Y. Tsay, F. Ukegawa, D. Underwood, S. Vejcik, R. Vidal, R. G. Wagner, R. L. Wagner, N. Wainer, J. Walsh, T. Watts, R. Webb, C. Wendt, H. Wenzel, W. C. Wester, T. Westhusing, S. N. White, A. B. Wicklund, H. H. Williams, B. L. Winer, J. Wyss, A. Yagil, K. Yasuoka, G. P. Yeh, J. Yoh, M. Yokoyama, J. C. Yun, A. Zanetti, F. Zetti, and S. Zucchelli, Phys. Rev. Lett., **68**, 2734 (1992). (CDF Collaboration)

[46] J. Badier, M. Bardadin-Otwinowska, C. Bemporad, U. Berthon, H. Bienvenu, J. Boucrot, J. Bourotte, G. Burgun, O. Callot, Ph. Charpentier, A. M. Cnops, M. Cohen, F. Constantini, M. Crozon, D. Décamp, P. Delpierre, J. F. Detoeuf, P. Espigat, B. Gandois, G. R. Giannini, V. Hajjar, M. Hansroul, Y. Karyotakis, P. Lariccia, P. Le Dû, J. Mas, A. Michelini, G. C. Moneti, M. Moniez, E. Paré, G. Rahal-Callot, M. Rumpf, O. Runolfsson, A. Tilquin, and S. Weisz, Z. Phys. **C31**, 341 (1986). (NA3 Collaboration)

[47] M. McLaughlin, J. Biel, C. Bromberg, B. Brown, C. Chandlee, S. Cihangir, S. R. W. Cooper, T. Ferbel, D. Garelick, G. Glass, M. Glaubman, S.-R. Han, K. Keller, S. Houssain, J. Huston, A. Jonckheere, J. LeBritton, R. A. Lewis, F. Lobkowicz, M. Marshak, C. A. Nelson, E. Peterson, E. Pothier, J. Povlis, K. Ruddick, M. Shupe, P. Slattery, and G. A. Smith, Phys. Rev. Lett. **51**, 971 (1983).

[48] G. Alverson, W. F. Baker, G. Ballocchi, R. Benson, D. Berg, S. Blusk, C. Bromberg, D. Brown, D. Carey, T. Chand, C. Chandlee, B. C. Choudhary, W. H. Chung, L. de Barbaro, W. De Soi, W. Dlugosz, J. Dunlea, S. Easo, E. Engels, W. Faissler, G. Fanourakis, T. Ferbel, D. Garelick, G. Ginther, G. Glass, M. Glaubman, P. Gutierrez, K. Hartman, J. Huston, C. Johnstone, V. Kapoor, I. Kourbanis, A. Lanaro, C. Lirakis, F. Lobkowicz, P. Lukens, S. Mani, A. Maul, J. Mansour, R. Miller, C. A. Nelson, B. Oh, D. Orris, E. Pothier, E. Prebys, B. M. Rajaram, R. Roser, K. Ruddick, P. Shepard, R. K. Shivpuri, A. Sinanidis, D. Skow, P. Slattery, L. Sorrell, W. Toothacker, N. Varelas, D. Weerasundara, J. Whitmore, G. Wu, T. Yasuda, C. Yosef, and M. Zieliński, Phys. Rev. Lett. **68**, 2584 (1992). (E706 collaboration)

[49] R. Bellwied, P. Braun-Munzinger, G. David, B. Hong, R. McGrath, J. Stachel, N. Xu, Y. C. Zhang, M. Zou, C. Woody, P. DeYoung, P. Gonthier, P. Jolivette, R. Arjaeinejad, J. Cole, M. Drigert, D. Struttmann, S. Y. Lee, T. Cormier, H. Dejbakhsh, S. Dutta, Q. Li, W. Trzaska and T. Hemmick, RHIC LOI #9 (Sept. 28, 1990), Fig. 2.

[50] C. Albajar, M. G. Albrow, O. C. Allkofer, B. Andrieu, K. Ankoviak, R. Apsimon, A. Astbury, B. Aubert, C. Bacci, T. Bacon, N. Bains, G. Bauer, S. Beingessner, A. Bettini, A. Bezaguet, P. Biddulph, H. Bohn, A. Böhrer, R. Bonino, K. Bos, M. Botlo, B. Buschbeck, G. Busetto, A. Caner, P. Casoli, F. Cavanna, P. Cennini, S. Centro, F. Ceradini, D. G. Charlton, G. Ciapetti, S. Cittolin, E. Clayton, D. Cline, J. Colas, P. Colas, R. Conte, J. A. Coughlan, G. Cox, D. Dau, J. P. Debrion, M. Degiorgi, M. Della Negra, M. Demoulin, D. Denegri, H. Dibon, A. Diciaccio, F. J. Diez Hedo, L. Dobrzynski, J. Dorenbosch, J. D. Dowell, K. Eggert, E. Eisenhandler, N. Ellis, P. Erhard, H. Faissner, I. F. Fensome, A. Ferrando, M. Fincke-Keeler, L. Fortson, T. Fuess, J. Garvey, S. Geer, A. Geiser, C. Ghiglino, Y. Giraud-Heraud,

A. Givernaud, A. Gonidec, J. M. Gregory, W. Haynes, D. J. Holthuizen, M. Ikeda, W. Jank, M. Jimack, G. Jorat, D. Joyce, P. I. P. Kalmus, V. Karimäki, R. Keeler, I. Kenyon, A. Kernan, A. Khan, W. Kienzle, R. Kinnunen, M. Krammer, J. Kroll, D. Kryn, F. Lacava, S. Lammel, M. Landon, R. Leuchs, S. Levegrün, M. Lindgren, D. Linglin, P. Lipa, C. Markou, M. Markytan, M. A. Marquina, G. Maurin, S. McMahon, J.-P. Mendiburu, A. Meneguzzo, J. P. Merlo, T. Meyer, T. Moers, M. Mohammadi, K. Morgan, H.-G. Moser, A. Moulin, B. Mours, Th. Muller, L. Naumann, P. Nedelec, M. Nikitas, A. Nisati, A. Norton, V. O'Dell, G. Pancheri, F. Pauss, E. Petrolo, G. Piano Mortari, E. Pietarinen, M. Pimiä, A. Placci, J.-P. Porte, M. Preischl, R. Prosi, E. Radermacher, T. Redelberger, H. Reithler, J.-P. Revol, D. Robinson, T. Rodrigo, J. Rohlf, C. Rubbia, G. Sajot, G. Salvini, J. Sass, D. Samyn, D. Schinzel, M. Schröder, A. Schwartz, W. Scott, C. Seez, T. P. Shah, I. Siotis, D. Smith, P. Sphicas, C. Stubenrauch, K. Sumorok, F. Szoncso, A. Taurok, L. Taylor, I. Ten Have, S. Tether, G. Thompson, E. Tscheslog, J. Tuominiemi, W. van de Guchte, A. van Dijk, S. Veneziano, J. P. Vialle, T. S. Virdee, W. von Schlippe, J. Vrana, V. Vuillemin, K. Wacker, G. Walzel, I. Wingerter, X. Wu, C.-E. Wulz, M. Yvert, C. Zaccardelli, I. Zacharov, L. Zanello, and P. Zotto, Nucl. Phys., **B335**, 261 (1990). (UA1 collaboration)

[51] C. De Marzo, M. De Palma, C. Favuzzi, G. Maggi, E. Nappi, F. Posa, A. Ranieri, G. Selvaggi, P. Spinelli, A. Bamberger, M. Fuchs, W. Heck, C. Loos, R. Marx, K. Runge, E. Skodzek, C. Weber, M. Wülker, F. Zetsche, V. Artemiev, Yu. Galaktionov, A. Gordeev, Yu. Gorodkov, Yu. Kamyshkov, M. Kossov, V. Plyaskin, V. Pojidaev, V. Shevchenko, E. Shumilov, V. Tchudakov, J. Bunn, J. Fent, P. Freund, J. Gebauer, M. Glas, P. Polakos, K. Pretzl, T. Schouten, P. Seyboth, J. Seyerlein, and G. Vesztergombi, Phys. Rev. **D36**, 16 (1987). (NA24 Collaboration)

[52] J. Antille, S. Baumann, A. Bernasconi, R. E. Breedon, L. Camilleri, R. L. Cool, P. T. Cox, L. Dick, E. C. Dukes, M. Duro, B. Gabioud, F. Gaille, P. Giacomelli, J. B. Jeanneret, C. Joseph, W. Kubischta, J. F. Loude, E. Malamud, C. Morel, O. E. Overseth, J. L. Pages, J. P. Perroud, P. Petersen, D. Ruegger, R. W. Rusack, G. R. Snow, G. Sozzi, D. Steiner, M. T. Tran, A. Vacchi, G. Valenti, and G. von Dardel, Phys. Lett. **194B**, 568 (1987). (UA6 Collaboration)

[53] A. L. S. Angelis, B. J. Blumenfeld, L. Camilleri, T. J. Chapin, R. L. Cool, C. del Papa, L. Di Lella, Z. Dimčovski, R. J. Hollebeek, L. M. Lederman, D. Levinthal, J. T. Linnemann, L. Lyons, N. Phinney, B. G. Pope, S. H. Pordes, A. F. Rothenberg, A. M. Segar, J. Singh-Sidhu, A. M. Smith, M. J. Tannenbaum, R. A. Vidal, J. Wallace-Hadrill, T. O. White, and J. M. Yelton, Phys. Lett. **79B**, 505 (1978). (CCOR - R110 Collaboration)

[54] A. L. S. Angelis, G. Basini, H. J. Besch, R. E. Breedon, L. Camilleri, T. J. Chapin, C. Chasman, R. L. Cool, P. T. Cox, Ch. von Gagern, C. Grosso-Pilcher, D. S. Hanna, P. E. Haustein, B. M. Humphries, J. T. Linnemann, C. B. Newman-Holmes, R. B. Nickerson, J. W. Olness, N. Phinney, B. G. Pope, S. H. Pordes, K. J. Powell, R. W. Rusack, C. W. Salgado, A. M. Segar, S. R. Stampke, M. Tanaka, M. J. Tannenbaum, P. Thieberger, and J. M. Yelton, Phys. Lett. **185B**, 213 (1987). (BCMOR - R110 Collaboration)

[55] F. Abe, D. Amidei, G. Apollinari, G. Ascoli, M. Atac, P. Auchincloss, A. R. Baden, A. Barbaro-Galtieri, V. E. Barnes, F. Bedeschi, S. Belforte, G. Bellettini, J. Bellinger, J. Bensinger, A. Beretvas, P. Berge, S. Bertolucci, S. Bhadra, M. Binkley, R. Blair, C. Blocker, J. Bofill, A. W. Booth, G. Brandenburg, D. Brown, A. Byon, K. L. Byrum, M. Campbell, R. Carey, W. Carithers, D. Carlsmith, J. T. Carroll, R. Cashmore, F. Cervelli, K. Chadwick, T. Chapin, G. Chiarelli, W. Chinowsky, S. Cihangir, D. Cline, D. Connor, M. Contreras, J. Cooper, M. Cordelli, M. Curatolo, C. Day, R. Del Fabbro, M. Dell'Orso, L. DeMortier, T. Devlin, D. DiBitonto, R. Diebold, F. Dittus, A. DiVirgilio, J. E. Elias, R. Ely, S. Errede, B. Esposito, A. Feldman, B. Flaugher, E. Focardi, G. W. Foster, M. Franklin, J. Freeman, H. Frisch, Y. Fukui, A. F. Garfinkel, P. Giannetti, N. Giokaris, P. Giromini, L. Gladney, M. Gold, K. Goulianos, C. Grosso-Pilcher, C. Haber, S. R. Hahn, R. Handler, R. M. Harris, J. Hauser, T. Hessing, R. Hollebeek, L. Holloway, P. Hu, B. Hubbard, P. Hurst, J. Huth, H. Jensen, R. P. Johnson, U. Joshi, R. W. Kadel, T. Kamon, S. Kanda, D. A. Kardelis, I. Karliner, E. Kearns, R. Kephart, P. Kesten, H. Keutelian, S. Kim, L. Kirsch, K. Kondo, U. Kruse, S. E. Kuhlmann, A. T. Laasanen, W. Li, T. Liss, N. Lockyer, F. Marchetto, R. Markeloff, L. A. Markosky, P. McIntyre, A. Menzione, T. Meyer, S. Mikamo, M. Miller, T. Mimashi, S. Miscetti, M. Mishina, S. Miyashita, N. Mondal, S. Mori, Y. Morita, A. Mukherjee, C. Newman-Holmes, L. Nodulman, R. Paoletti, A. Para, J. Patrick, T. J. Phillips, H. Piekarz, R. Plunkett, L. Pondrom, J. Proudfoot, G. Punzi, D. Quarrie, K. Ragan, G. Redlinger, J. Rhoades, F. Rimondi, L. Ristori, T. Rohaly, A. Roodman, A. Sansoni, R. Sard, V. Scarpine, P. Schlabach, E. E. Schmidt, P. Schoessow, M. H. Schub, R. Schwitters, A. Scribano, S. Segler, M. Sekiguchi, P. Sestini, M. Shapiro, M. Sheaff, M. Shibata, M. Shochet, J. Siegrist, P. Sinervo, J. Skarha, D. A. Smith, F. D. Snider, R. St. Denis, A. Stefanini, Y. Takaiwa, K. Takikawa, S. Tarem, D. Theriot, A. Tollestrup, G. Tonelli, Y. Tsay, F. Ukegawa, D. Underwood, R. Vidal, R. G. Wagner, R. L. Wagner, J. Walsh, T. Watts, R. Webb, T. Westhusing, S. White, A. Wicklund, H. H. Williams, T. Yamanouchi, A. Yamashita, K. Yasuoka, G. P. Yeh, J. Yoh, and F. Zetti, Phys. Rev. Lett., **61**, 1819 (1988). (CDF Collaboration)

[56] "Conceptual Design of the Relativistic Heavy Ion Collider RHIC", Brookhaven National Laboratory Report BNL 52195, (1989), unpublished.

[57] T. W. Ludlam and N. P. Samios, Z. Phys., **C38**, 353 (1988); T. Ludlam, American Institute of Physics Conference Proceedings, **223**, 139 (1991) (Penn. State meeting); and T. Ludlam, private communication.

[58] G. Bunce, American Institute of Physics Conference Proceedings, **223**, 147 (1991). (Penn. State meeting)

[59] E. Eichten, I. Hinchcliffe, K. Lane, and C. Quigg, Rev. Mod. Phys. **56**, 579 (1984); erratum **58**, 1065 (1986).

[60] Yung-Su Tsai, Rev. Mod. Phys., **46** (1974) 815.

TABLE 1: Input data for fits to measured direct-γ production cross sections. In some cases, numerical values were not given in the published paper, and these values were read from the graphs of data. The P_T and η ranges for the data and/or fits are shown, along with the reaction studied.

$\sqrt{s}(GeV)$	$P_{T,\gamma}$ (GeV/c)	Reaction	Range	Ref.
19.4	2.7 - 4.5	$pC \rightarrow \gamma X$	$-0.75 \leq \eta \leq +0.2$	McLaughlin et al. [47]
19.4	3.9 - 5.0	$pC \rightarrow \gamma X$	$-0.4 \leq \eta \leq +0.8$	Badier et al. [46]
23.0	4.1 - 6.2	$pp \rightarrow \gamma X$	$\|x_F\| \leq 0.45$	Bonesini et al. [39]
23.8	3.2 - 6.0	$pp \rightarrow \gamma X$	$-0.6 \leq \eta \leq +0.5$	De Marzo et al. [38]
24.3	3.4 - 6.3	$p\overline{p} \rightarrow \gamma X$	$\langle\eta\rangle = 0.4$	Bernasconi et al. [40]
30.7	4.1 - 7.2	$pBe \rightarrow \gamma X$	$\|\eta\| \leq 0.7$	Alverson et al. [48]
62.4	6.3 - 12.3	$pp \rightarrow \gamma X$	$\|\eta\| \leq 0.7$	Angelis et al. [41]
63.0	3.7 - 11.5	$pp \rightarrow \gamma X$	$\|\eta\| \leq 0.35$	Anassontzis et al. [42]
546.	17. - 46.	$p\overline{p} \rightarrow \gamma X$	$\|\eta\| \leq 0.8$	Albajar et al. [44]
630.	17. - 35.	$p\overline{p} \rightarrow \gamma X$	$\|\eta\| \leq 0.8$	Albajar et al. [44]
630.	15. - 32.	$p\overline{p} \rightarrow \gamma X$	$\|\eta\| \leq 0.8$	Ansari et al. [43]
1800.	14.5 - 37.2	$p\overline{p} \rightarrow \gamma X$	$\|\eta\| \leq 1.0$	Abe et al. [45]

TABLE 2: Results of fits to measured inclusive direct-γ production cross sections. Cross sections involving nuclear targets are expressed per nucleon in the table. The values B and b correspond to Eq. 18 in the text, and σ_γ to Eq. 19. The inclusive direct-γ production cross section at $P_T = 10$ GeV/c is also tabulated. At lower $\sqrt{s}$ values, the data only yield limits to σ_γ. The $p\overline{p}$ results have NOT been divided by a factor of 1.3 to convert to the corresponding pp values in this table.

$\sqrt{s}(GeV)$	B (nb/GeV^2)	b (/GeV)	Ed$^3\sigma$/dP^3 (pb/GeV^2)	σ_γ (pb)	R
19.4	3700 ± 3900	2.51 ± 0.30	0.000046 ± 0.000093	0.0024 ± 0.0049	[4
19.4	1400 ± 2100	2.59 ± 0.34	0.000008 ± 0.000015	0.00040 ± 0.00077	[4
23.0	580 ± 690	2.34 ± 0.25	0.000042 ± 0.000056	0.0024 ± 0.0032	[3
23.8	350 ± 320	2.18 ± 0.20	0.000117 ± 0.000126	0.0070 ± 0.0075	[3
24.3	4600 ± 2100	2.53 ± 0.11	0.000048 ± 0.000032	0.0025 ± 0.0017	[4
30.7	2500 ± 2200	2.34 ± 0.18	0.000177 ± 0.000159	0.0099 ± 0.0089	[4
62.4	0.80 ± 0.46	0.73 ± 0.06	0.549 ± 0.058	108 ± 15	[4
63.0	117 ± 35	1.25 ± 0.04	0.432 ± 0.055	46.8 ± 6.2	[4
546.	0.200 ± 0.075	0.244 ± 0.018	17.5 ± 3.6	10800 ± 2400	[4
630.	0.382 ± 0.121	0.258 ± 0.013	28.9 ± 5.6	16900 ± 3400	[4
630.	0.860 ± 0.183	0.300 ± 0.010	42.8 ± 4.9	21800 ± 4300	[4
1800.	0.98 ± 0.28	0.262 ± 0.013	71.3 ± 11.3	41200 ± 7000	[4

TABLE 3: Input data for fits to measured π production cross sections. In some cases, numerical values were not given in the published paper, and these values were read from the graphs of data. The P_T and η ranges for the data and/or fits are shown, along with the reaction studied.

$\sqrt{s}(GeV)$	P_{T,π^0} (GeV/c)	Reaction	Range	Ref.
23.8	4.1 - 6.7	$pp \rightarrow \pi^0 X$	$-0.6 \leq \eta \leq +0.5$	De Marzo et al. [51]
24.3	2.0 - 4.8	$p\overline{p} \rightarrow \pi^0 X$	$\langle\eta\rangle = 0.4$	Antille et al. [52]
30.7	4.2 - 6.7	$pp \rightarrow \pi^0 X$	$\|\eta\| \leq 0.7$	Angelis et al. [53]
31.	3.4 - 8.4	$pp \rightarrow \pi^0 X$	$\|\eta\| \leq 0.55$	Angelis et al. [54]
53.1	3.7 - 12.7	$pp \rightarrow \pi^0 X$	$\|\eta\| \leq 0.7$	Angelis et al. [53]
62.4	3.7 - 13.7	$pp \rightarrow \pi^0 X$	$\|\eta\| \leq 0.7$	Angelis et al. [53]
63.0	3.6 - 11.5	$pp \rightarrow \pi^0 X$	$\|\eta\| \leq 0.35$	Anassontzis et al. [42]
200.	0.25 - 6.7	$p\overline{p} \rightarrow \pi^{\pm} X$	$\|\eta\| \leq 2.5$	Albajar et al. [50]
260.	0.25 - 6.7	$p\overline{p} \rightarrow \pi^{\pm} X$	$\|\eta\| \leq 2.5$	Albajar et al. [50]
380.	0.25 - 6.7	$p\overline{p} \rightarrow \pi^{\pm} X$	$\|\eta\| \leq 2.5$	Albajar et al. [50]
500.	0.25 - 7.3	$p\overline{p} \rightarrow \pi^{\pm} X$	$\|\eta\| \leq 2.5$	Albajar et al. [50]
620.	0.25 - 7.3	$p\overline{p} \rightarrow \pi^{\pm} X$	$\|\eta\| \leq 2.5$	Albajar et al. [50]
630.	0.4 - 10.	$p\overline{p} \rightarrow \pi^{\pm} X$	$\|\eta\| \leq 1.0$	Abe et al. [55]
790.	0.25 - 7.3	$p\overline{p} \rightarrow \pi^{\pm} X$	$\|\eta\| \leq 2.5$	Albajar et al. [50]
900.	0.25 - 9.2	$p\overline{p} \rightarrow \pi^{\pm} X$	$\|\eta\| \leq 2.5$	Albajar et al. [50]
1800.	0.4 - 10.	$p\overline{p} \rightarrow \pi^{\pm} X$	$\|\eta\| \leq 1.0$	Abe et al. [55]

TABLE 4: Results of fits to measured inclusive π production cross sections. The values A, p_0 and N correspond to Eq. 20 in the text. The $p\overline{p}$ results have NOT been modified to convert to the corresponding pp values in this table. Note that A increases rapidly as p_0 decreases.

$\sqrt{s}(GeV)$	A (mb/GeV^2)	p_0 (GeV/c)	N	Ref.
23.8	301 ± 92	3.46 ± 0.37	25.2 ± 1.5	[51]
24.3	89 ± 125	4.9 ± 2.2	30.3 ± 8.2	[52]
30.7	22 ± 40	2.9 ± 1.7	18.3 ± 4.1	[53]
31.	3.9 ± 7.1	5.0 ± 2.0	23.5 ± 5.0	[54]
53.1	3700 ± 2800	1.07 ± 0.35	12.23 ± 0.59	[53]
62.4	17 ± 14	2.06 ± 0.38	12.65 ± 0.42	[53]
63.0	$1.06 \times 10^5 \pm 1.91 \times 10^7$	0.82 ± 0.39	12.65 ± 0.76	[42]
200.	286 ± 17	1.80 ± 0.10	12.14 ± 0.39	[50]
260.	230 ± 19	1.85 ± 0.12	12.15 ± 0.50	[50]
380.	362 ± 23	1.53 ± 0.09	10.51 ± 0.35	[50]
500.	408 ± 24	1.61 ± 0.08	10.64 ± 0.31	[50]
620.	382 ± 22	1.54 ± 0.08	10.24 ± 0.28	[50]
630.	270 ± 10	1.63 ± 0.13	10.20 ± 0.56	[55]
790.	390 ± 20	1.53 ± 0.06	10.16 ± 0.23	[50]
900.	382 ± 20	1.56 ± 0.05	9.96 ± 0.17	[50]
1800.	450 ± 10	1.29 ± 0.02	8.26 ± 0.08	[55]

TABLE 5: Predictions from fits to measured inclusive π production cross sections. The inclusive π^0 production cross section at $P_T = 10$ GeV/c is tabulated assuming there are no differences between $p\overline{p}$ and pp results or between π^0 and $\pi^{\pm}$. The value of σ_{π^0} from Eq. 21 is also given. In many cases, the quoted uncertainties are only estimates.

$\sqrt{s}(GeV)$	$\mathrm{E}\mathrm{d}^3\sigma/\mathrm{d}P^3$ (pb/GeV^2)	σ_{π^0} (pb)	Ref.
23.8	0.00041 ± 0.00013	0.030 ± 0.011	[51]
24.3	0.00020 ± 0.00028	0.014 ± 0.022	[52]
30.7	0.029 ± 0.013	3.0 ± 1.6	[53]
31.	0.024 ± 0.010	2.2 ± 1.1	[54]
53.1	1.26 ± 0.03	180. ± 8.	[53]
62.4	3.21 ± 0.03	463. ± 10.	[53]
63.0	0.93 ± 0.06	120. ± 11.	[42]
200.	35 ± 7	5200 ± 1200	[50]
260.	36 ± 7	5400 ± 1300	[50]
380.	220 ± 44	38000 ± 9000	[50]
500.	300 ± 60	61000 ± 14000	[50]
620.	420 ± 70	75000 ± 14000	[50]
630.	530 ± 100	100000 ± 25000	[55]
790.	480 ± 60	86000 ± 14000	[50]
900.	830 ± 80	153000 ± 17000	[50]
1800.	7400 ± 700	1700000 ± 200000	[55]

TABLE 6: Calculation of N_γ and δA_{LL} for an ideal detector at three values of $\sqrt{s}$. The cross sections σ_γ and σ_{π^0} are interpolated from Fig. 5, and the luminosities are taken from Fig. 7. A one month run at 100% efficiency and beam polarizations of 0.7 are assumed.

$\sqrt{s}$	100 GeV	200 GeV	500 GeV
Time (Δt)	2.59×10^6 sec	2.59×10^6 sec	2.59×10^6 sec
σ_γ	250 pb	1080 pb	8000 pb
σ_{π^0}	1000 pb	5200 pb	60000 pb
Design Luminosity	2.8×10^{30} /cm^2/sec	5.6×10^{30} /cm^2/sec	1.4×10^{31} /cm^2/sec
N_γ	1.81×10^3	1.57×10^4	2.90×10^5
δA_{LL}	±0.048	±0.016	±0.0038
High Luminosity	4.0×10^{31} /cm^2/sec	8.0×10^{31} /cm^2/sec	2.0×10^{32} /cm^2/sec
N_γ	2.59×10^4	2.24×10^5	4.15×10^6
δA_{LL}	±0.013	±0.0043	±0.0010

TABLE 7: ISAJET cross sections for direct-γ over various kinematic regions. In left portion of table no restrictions were imposed on jets opposite direct-γ. In right portion of table rapidity cuts are made on the jets, for direct-γ $|\eta| \leq 1$. Cross sections have estimated errors on the 5% level.

$P_{T,\gamma}$ range	η_γ range	σ_γ	η_{jet} range	$\sigma_{\gamma,jet}$
5 to 10	$-.3$ to $+.3$	3813 pb	$-.3$ to $+.3$	2630 pb
	-1 to $+1$	11864 pb	-1 to $+1$	7615 pb
10 to 15	$-.3$ to $+.3$	241 pb	$-.3$ to $+.3$	200 pb
	-1 to $+1$	732 pb	-1 to $+1$	555 pb
15 to 20	$-.3$ to $+.3$	31 pb	$-.3$ to $+.3$	28 pb
	-1 to $+1$	87 pb	-1 to $+1$	73 pb

TABLE 8: The expected numbers of $pp \to \gamma + \text{jet} + X$ events as a function of $\sqrt{s}$, with $x_b \geq 0.2$. This includes half the available kinematic region shaded in Fig. 20. The P_T interval was 10–20 GeV/c, with acceptances $|\eta_\gamma| \leq 2$ and $|\eta_{jet}| \leq 1.3$. For each ISAJET run ($\mathcal{N}_{tot}$ events in acceptance, n_a events with $x_b \geq 0.2$), the equivalent integral luminosity ($\int Ldt$) was recorded and used in conjunction with the RHIC design luminosity to scale n_a for 1-RHIC-month running at each energy. The mean of the x_a distribution and its width is also tabulated for each $\sqrt{s}$.

$\sqrt{s}$	$\mathcal{N}_{tot}$	$\int Ldt$	n_a	$\int_{RHIC} Ldt$	n_a/month	$\langle x_a \rangle$	σ_{RMS}
50	10^4	.2836 E+13	9994	.3626 E+10	13	.467	.134
100	·	.4487 E+11	6597	.7252 E+10	1066	.212	.096
150	·	.1263 E+11	4288	.1088 E+11	3693	.120	.061
200	·	.6631 E+10	2921	.1450 E+11	6389	.078	.044
250	·	.4480 E+10	2100	.1813 E+11	8498	.056	.035
300	·	.3416 E+10	1393	.2176 E+11	8872	.043	.028
350	10^5	.2770 E+11	9855	.2538 E+11	9030	.034	.020
400	·	.2358 E+11	6633	.2901 E+11	8160	.028	.016
450	·	.2066 E+11	4440	.3263 E+11	7013	.024	.014
500	·	.1850 E+11	2917	.3626 E+11	5717	.021	.013

TABLE 9: Estimates of δA_{LL} for various x regions at $\sqrt{s} = 200$ GeV. The first column lists the binning for $x_a = \min(x_1, x_2)$, while the remaining columns are bins for $x_b = \max(x_1, x_2)$. An ideal detector with acceptances $|\eta_\gamma| \leq 2$, $|\eta_{jet}| \leq 1.3$, $P_T \geq 10$ GeV/c was assumed. Errors listed have been scaled for 1-RHIC-month and normalized with polarization $P_B = 0.7$. The output ISAJET total cross section was 1894 pb.

		$\max(x_1, x_2)$			
	$\min(x_1, x_2)$	$\leq$0.2	0.2–0.3	0.3–0.4	>0.4
Design Luminosity $\int_{RHIC} Ldt = 0.1450 \times 10^{11}$/mb	0.00–0.05		0.058	0.043	0.036
	0.05–0.10	0.029	0.029	0.044	0.058
	0.10–0.15	0.033	0.051	0.095	0.145
	0.15–0.20	0.099	0.085	0.178	0.283
	>0.20		0.165	0.230	0.343
		$\max(x_a, x_b)$			
	$\min(x_a, x_b)$	$\leq$0.2	0.2–0.3	0.3–0.4	>0.4
Enhanced Luminosity $\int_{RHIC} Ldt = 0.2072 \times 10^{12}$/mb	0.00–0.05		0.015	0.011	0.009
	0.05–0.10	0.008	0.008	0.012	0.015
	0.10–0.15	0.009	0.013	0.025	0.038
	0.15–0.20	0.026	0.023	0.047	0.075
	>0.20		0.044	0.061	0.091

TABLE 10: Form of the error factor $\mathcal{Q}_{max}$ for various direct-γ detection schemes.

scheme	$\mathcal{Q}_{max}$	
ideal detector	1	
π° reconstruction	$\begin{cases} \left[1 + \Gamma + \frac{\Gamma^2}{1-\Gamma} P_B^4\right]^{\frac{1}{2}} & \text{if } \Gamma \leq \frac{1}{2} \\ \left[1 + \Gamma + (3\Gamma - 1) P_B^4\right]^{\frac{1}{2}} & \text{if } \Gamma \geq \frac{1}{2} \end{cases}$	; $\Gamma = R_{fake} \frac{N_{\pi^\circ}}{N_\gamma}$
preshower/preconvertor	$\left[\frac{(1-P_B^4)}{2}\left[4\sqrt{X+1} + X + 6\right]\right]^{\frac{1}{2}}$ if $\nu > \nu_{critical}$ (see text)	; $X = 2\frac{N_{\pi^\circ}}{N_\gamma}\frac{1+3P_B^4}{1-P_B^4}$

Figures

FIG. 1. Parton distributions as functions of x for u valence quarks, gluons, and sea $\bar{u}$ quarks). The forms of these distributions were taken from EHLQ (Ref. 59) at $Q^2 \sim 5$ (GeV/c)^2.

FIG. 2. Parton level cross sections for the Compton and annihilation subprocesses as functions of θ (c.m.). (a)Unpolarized or spin averaged cross sections are proportional to $|M|^2$ and spin dependent cross sections to $|\Delta M|^2$. (b)Parton level asymmetries $\hat{a}_{LL}$.

FIG. 3. Measured values of $A_1(x)$ (proportional to $g_1(x)$) and derived $xg_1(x)$, from SLAC and EMC experiments, as a function of x (Figures from Refs. 4,5).

FIG. 4. Parameters for fits to the inclusive direct-γ cross section as functions of $\sqrt{s}$ from Table 2. (a)The cross section at $P_T = 10$ GeV/c. (b)The slope b from Eq. 18.

FIG. 5. Estimated total direct-γ and π^0 cross sections for P_T between 10 and 20 GeV/c as functions of $\sqrt{s}$.

FIG. 6. Parameters for fits to the inclusive π cross sections as functions of $\sqrt{s}$ from Tables 4 and 5. (a)The cross section at $P_T = 10$ GeV/c. (b)The parameter p_0 from Eq. 20. (c)The parameter N from Eq. 20.

FIG. 7. The design and enhanced RHIC pp luminosity as functions of $\sqrt{s}$.

FIG. 8. ISAJET inclusive cross section for direct-γ + jet. The cross section goes roughly as P_T^{-6}.

FIG. 9. Energy deposited into polystyrene as a function of radial distance.

FIG. 10. The quantity $Q = P_B^2 \cdot \sqrt{N_\gamma} \cdot \delta A_{LL}$ as a function of Γ for the π°-reconstruction scheme.

FIG. 11. Ratio of fake-γ's to reconstructed π^0's (R_{fake}) for the PHENIX detector.

FIG. 12. R_{fake} ratio for fake photons for a model strip detector placed at a depth near shower maximum in the EM calorimeter. Three $R\Delta\phi$ values are shown ($R\Delta\phi \geq 1$ cm corresponds to 0.5 cm strips, etc.).

FIG. 13. Preshower/Calorimeter configuration for photon detection. The photon is assumed to enter from the left.

FIG. 14. The quantity $P_B^2 \cdot \sqrt{N_\gamma} \cdot \delta A_{LL}$ as a function of single-photon nonconversion probability ν_γ.

FIG. 15. Optimum preshower absorber thickness (radiation lengths $X_\circ$) and corresponding δA_{LL} as functions of the beam polarization P_B.

FIG. 16. A schematic representation of parton-parton scattering to define the scattering angle θ.

FIG. 17. The range of x_a (parton momentum fraction) corresponding to a barrel calorimeter with P_T cutoffs at 10 and 20 GeV/c.

FIG. 18. The range of x_a corresponding to a barrel and endcap calorimeter with P_T cutoffs (a) at 10, and (b) at 20 GeV/c. The three shaded regions represent $x_b \geq 0.2, 0.25, 0.3$ cuts.

FIG. 19. Plots of x_1 and x_2 as functions of the direct-γ and jet pseudorapidities. The solid lines represent contours for x_1 and the dashed lines are contours for x_2.

FIG. 20. Plot of the regions (shaded) where x_b is larger than 0.2, which corresponds to a sizeable quark polarization.

FIG. 21. Plot of data in Table 8: a) shows expected n_a for one month's running at design luminosity as a function of $\sqrt{s}$. The plateau near 200 GeV is due to the exponential fall off of $n_a/\mathcal{N}_{tot}$. b) mean of x_a distribution and its width as function of $\sqrt{s}$.

FIG. 22. The histogram shows the x_a distribution from an ISAJET simulation at $\sqrt{s}$=200 GeV using $|\eta_\gamma| \leq 2$, $|\eta_{jet}| \leq 1.3$, $10 \leq P_T \leq 20$ GeV/c, and requiring $x_b \geq 0.2$. The curve is a fit using the Johnson distribution S_B for bounded variables.

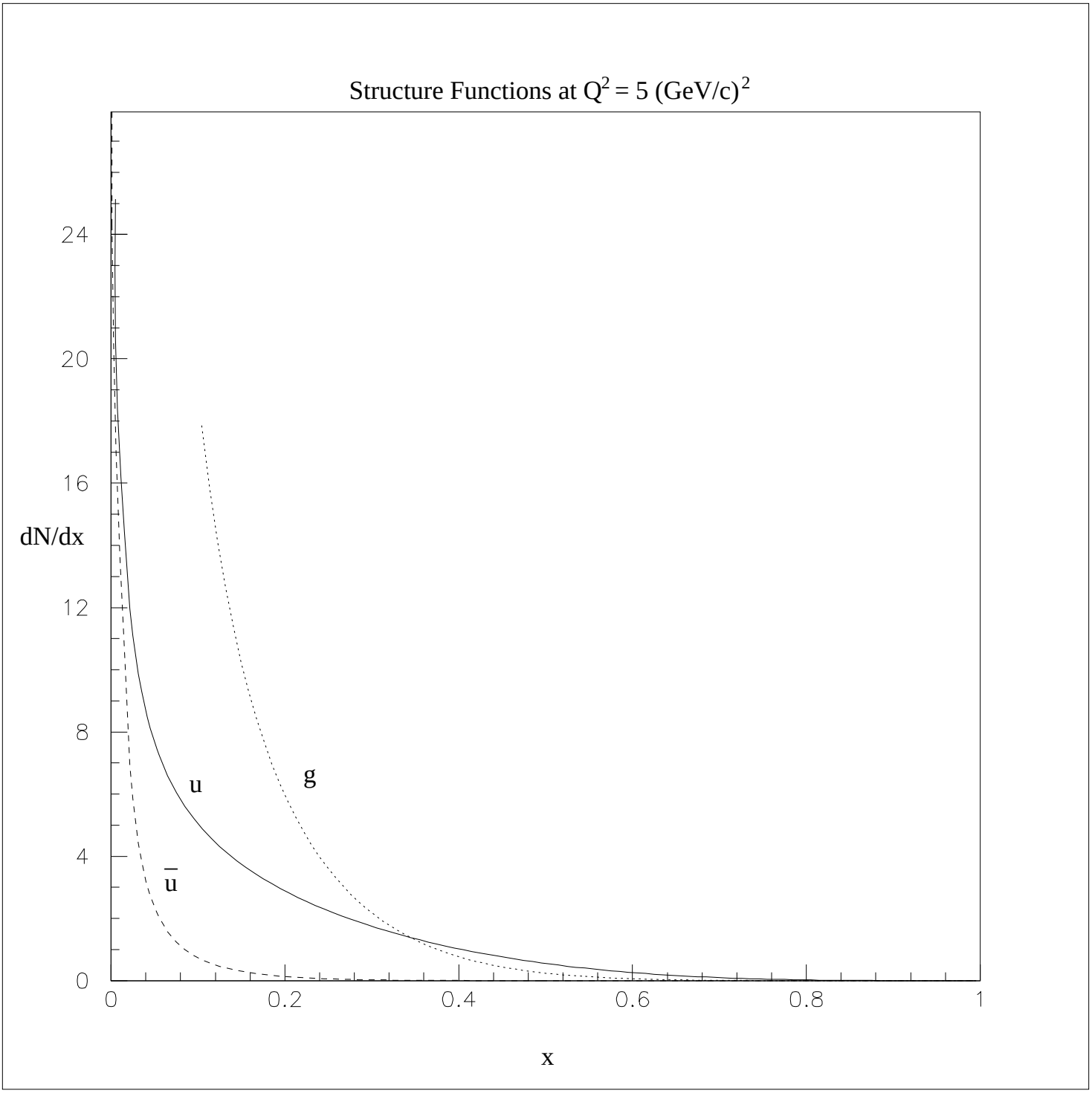
Structure Functions at $Q^2 = 5$ (GeV/c)^2
24
20
16
dN/dx
12
8
4
0
0
0.2
0.4
0.6
0.8
1
x
u
g
$\bar{u}$

Fig. 1

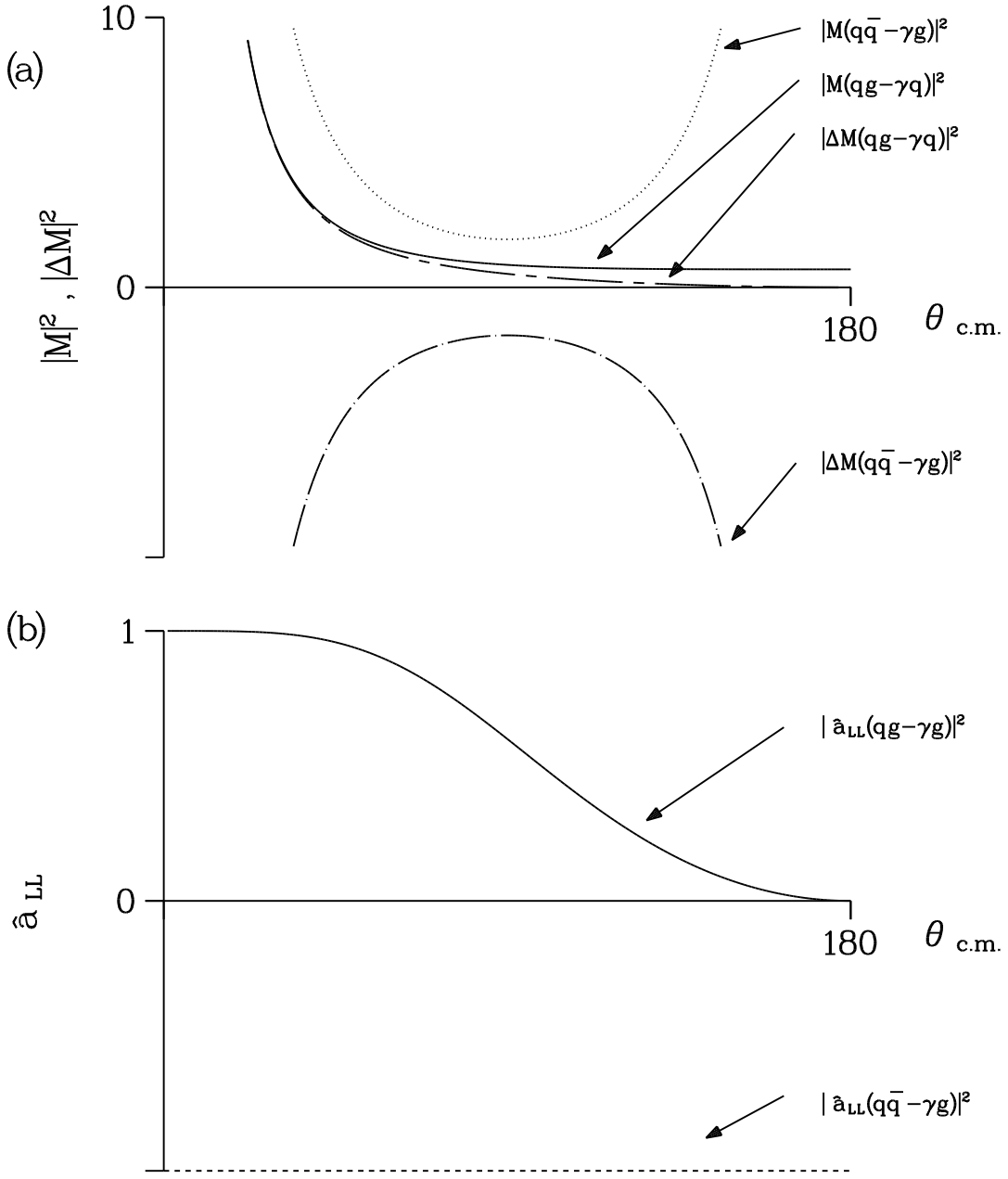
(a)
10
0
$|M|^2$, $|\Delta M|^2$
$|M(q\bar{q}-\gamma g)|^2$
$|M(qg-\gamma q)|^2$
$|\Delta M(qg-\gamma q)|^2$
180
θ c.m.
$|\Delta M(q\bar{q}-\gamma g)|^2$
(b)
1
0
$\hat{a}_{LL}$
$|\hat{a}_{LL}(qg-\gamma g)|^2$
180
θ c.m.
$|\hat{a}_{LL}(q\bar{q}-\gamma g)|^2$

Fig. 2

Fig. 3

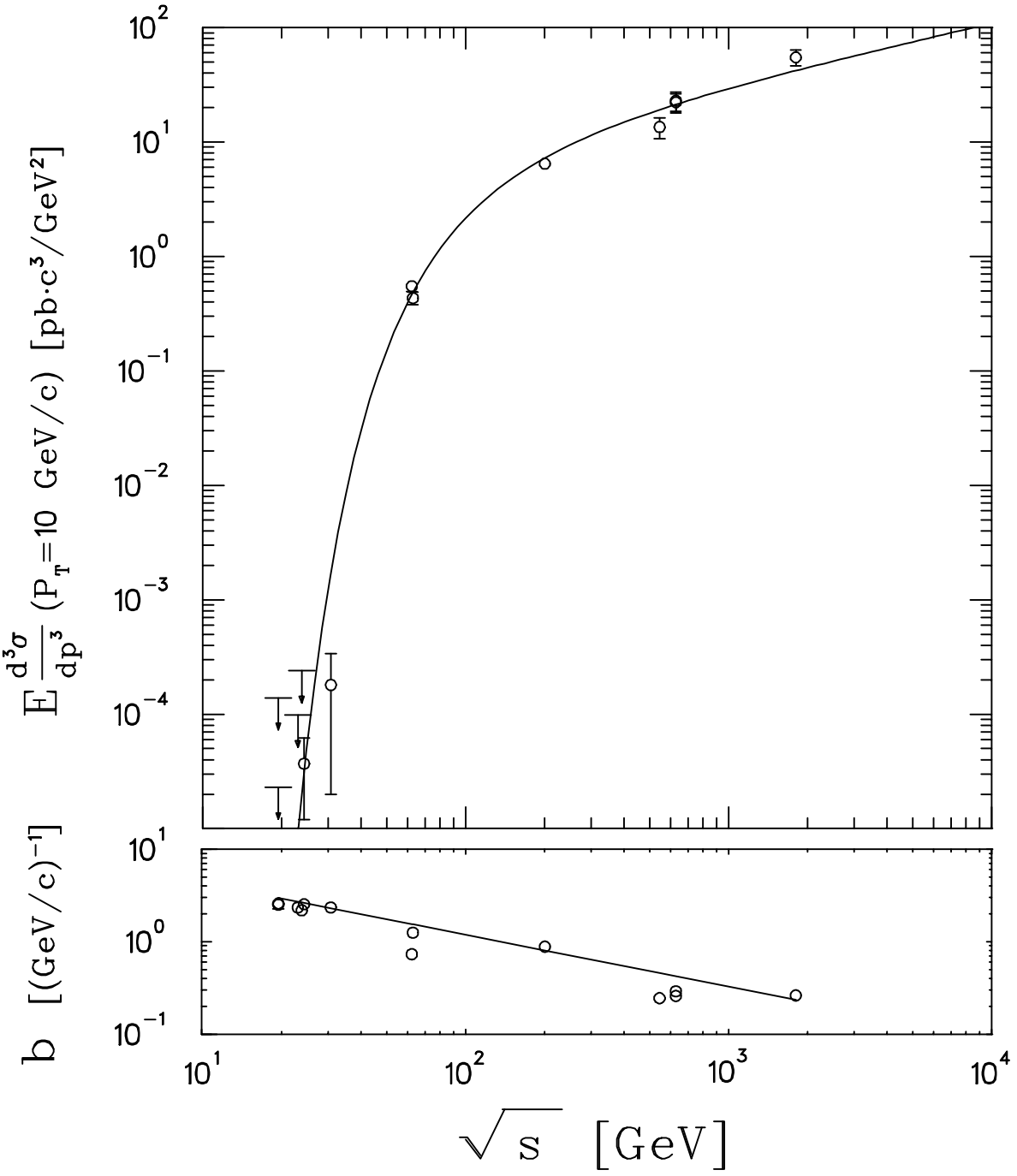

Fig. 4

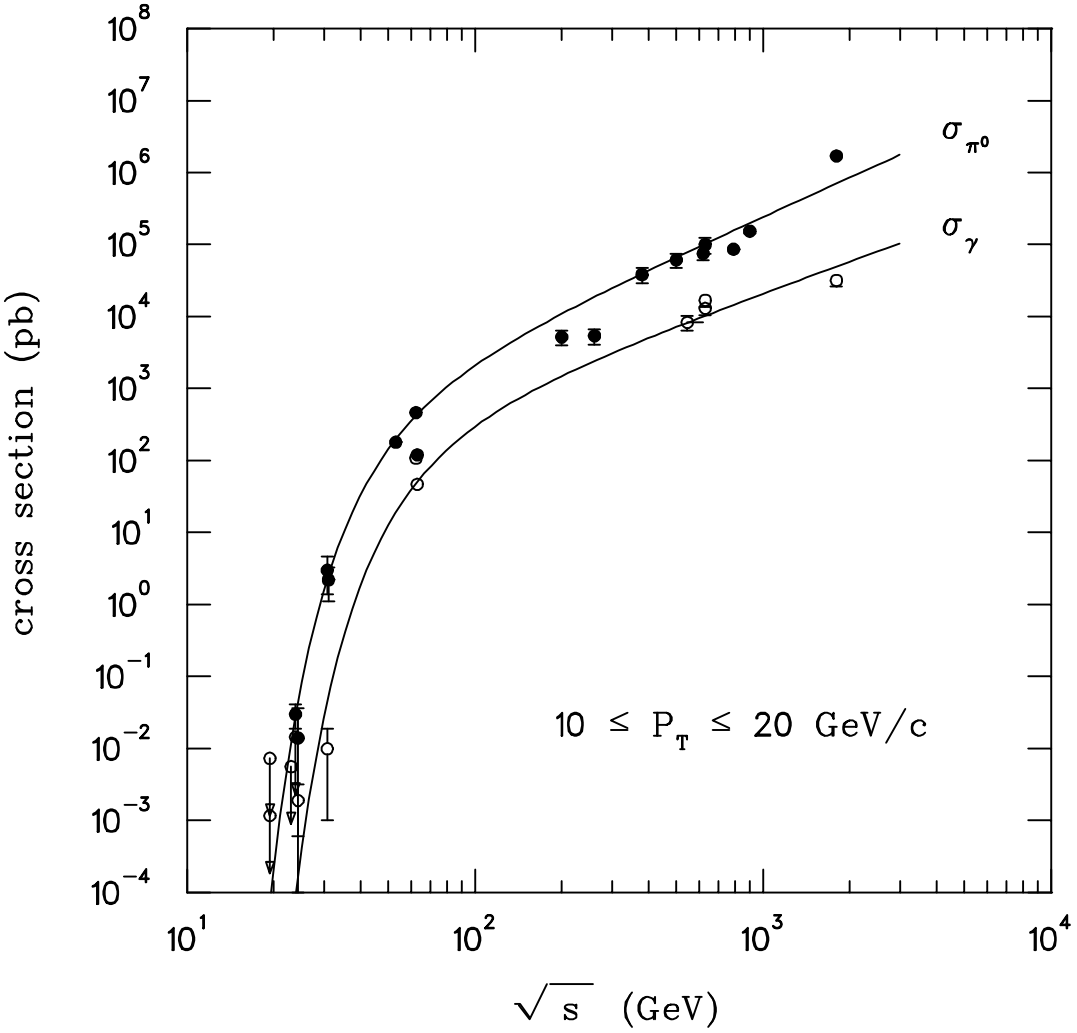
cross section (pb)
10^8
10^7
10^6
10^5
10^4
10^3
10^2
10^1
10^0
10^{-1}
10^{-2}
10^{-3}
10^{-4}
10^1
10^2
10^3
10^4
$\sqrt{s}$ (GeV)
σ_{π^0}
σ_γ
$10 \leq P_T \leq 20$ GeV/c

Fig. 5

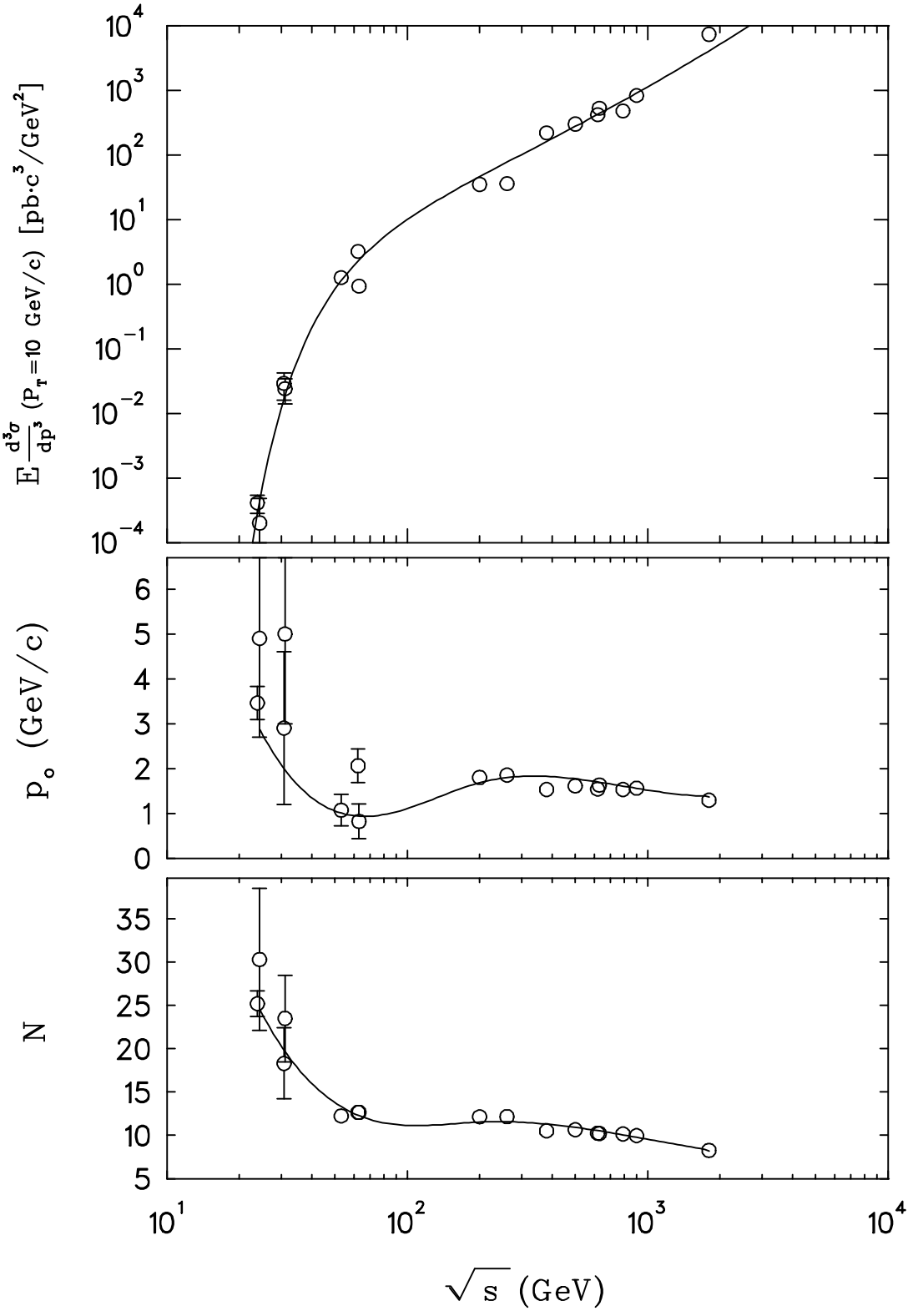
$E\frac{d^3\sigma}{dp^3}(P_T=10\ GeV/c)\ [pb\cdot c^3/GeV^2]$
10^4
10^3
10^2
10^1
10^0
10^{-1}
10^{-2}
10^{-3}
10^{-4}
p_o (GeV/c)
6
5
4
3
2
1
0
N
35
30
25
20
15
10
5
10^1
10^2
10^3
10^4
$\sqrt{s}$ (GeV)

Fig. 6

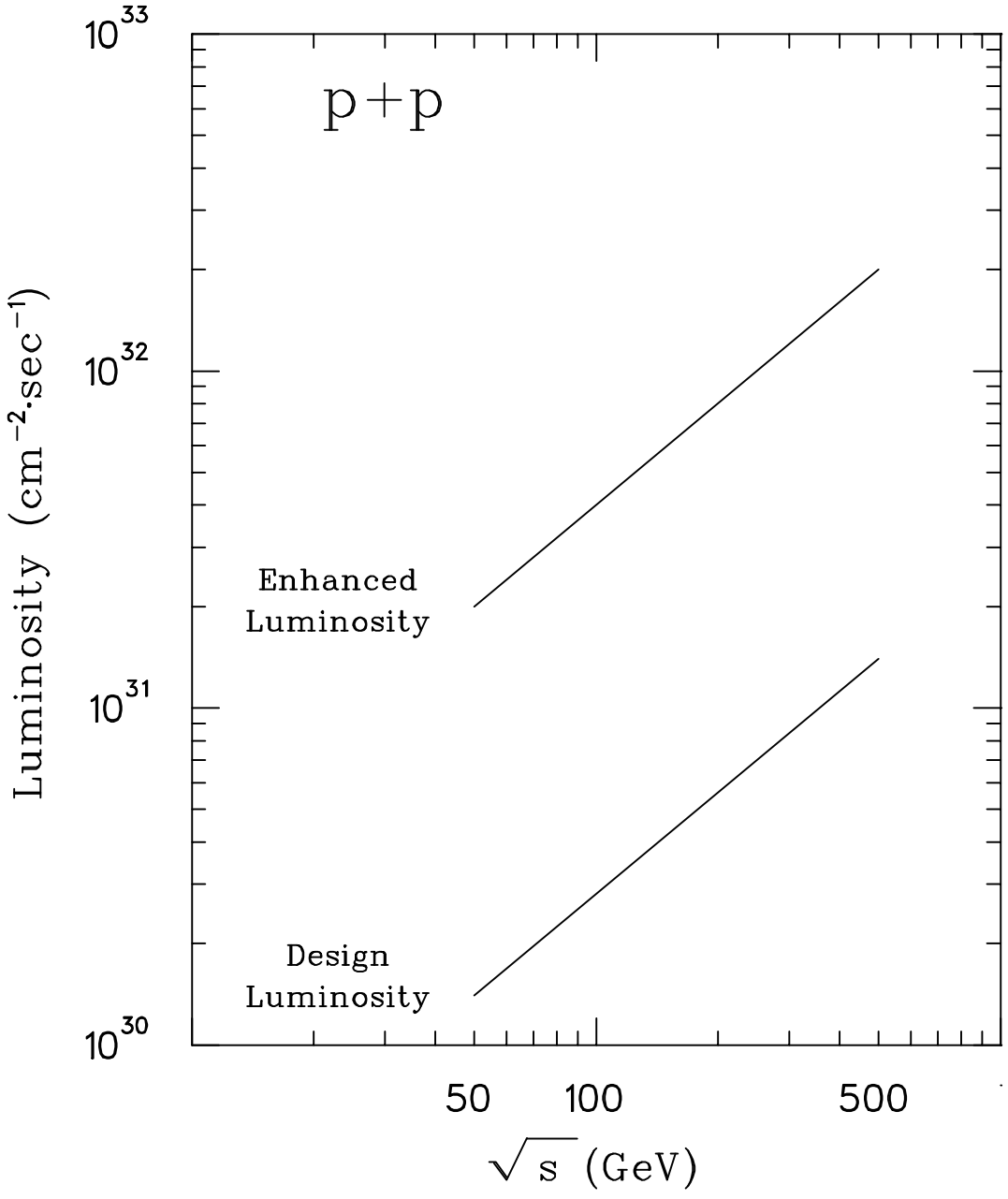
p+p
Enhanced
Luminosity
Design
Luminosity
Luminosity (cm^{-2}.sec^{-1})
10^{33}
10^{32}
10^{31}
10^{30}
50
100
500
$\sqrt{s}$ (GeV)

Fig. 7

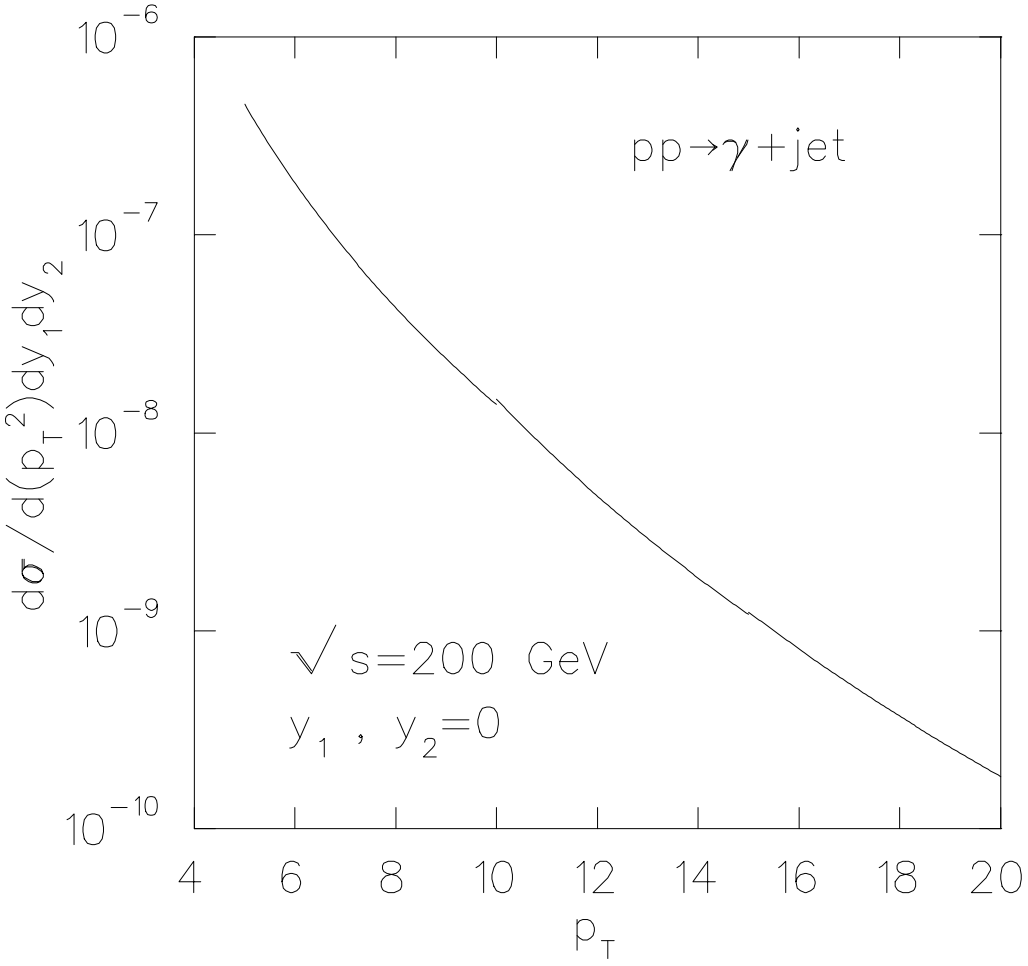
10^{-6}
10^{-7}
10^{-8}
10^{-9}
10^{-10}
$d\sigma / d(p_T^2) dy_1 dy_2$
$pp \rightarrow \gamma + jet$
$\sqrt{s} = 200$ GeV
$y_1 , y_2 = 0$
4
6
8
10
12
14
16
18
20
p_T

Fig. 8

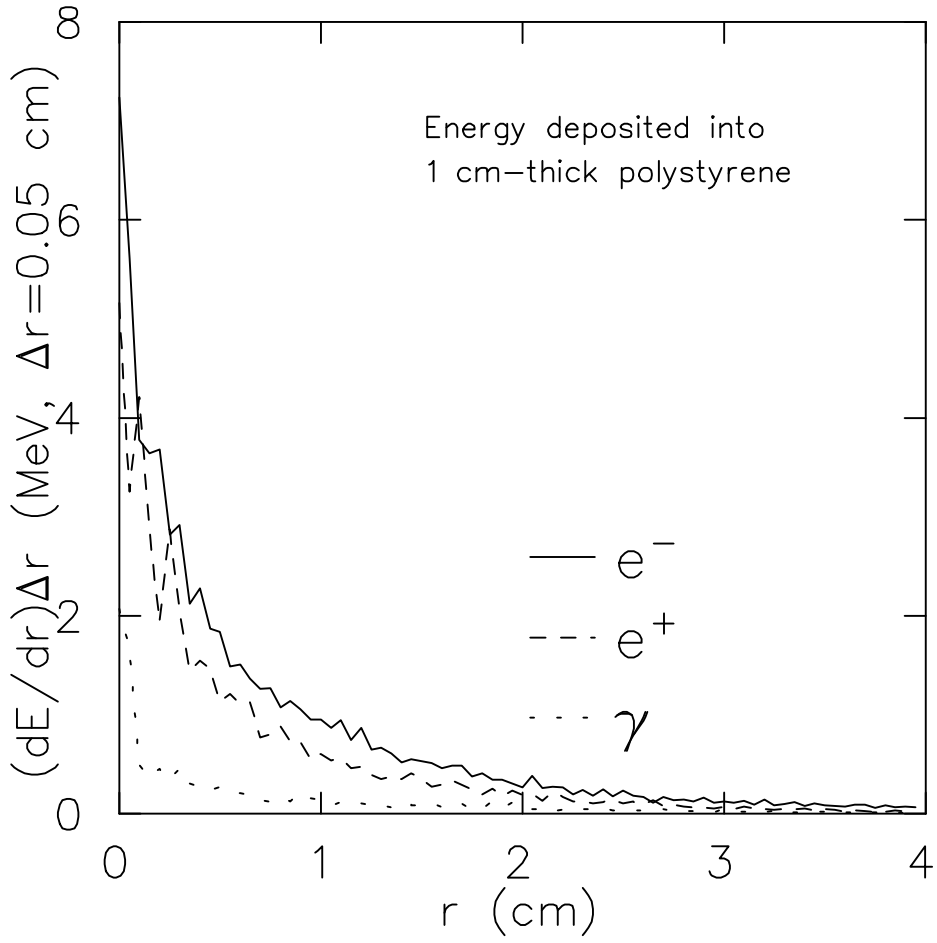
Energy deposited into
1 cm–thick polystyrene
e⁻
e⁺
γ
(dE/dr)Δr (MeV, Δr=0.05 cm)
r (cm)
0
2
4
6
8
0
1
2
3
4

Fig. 9

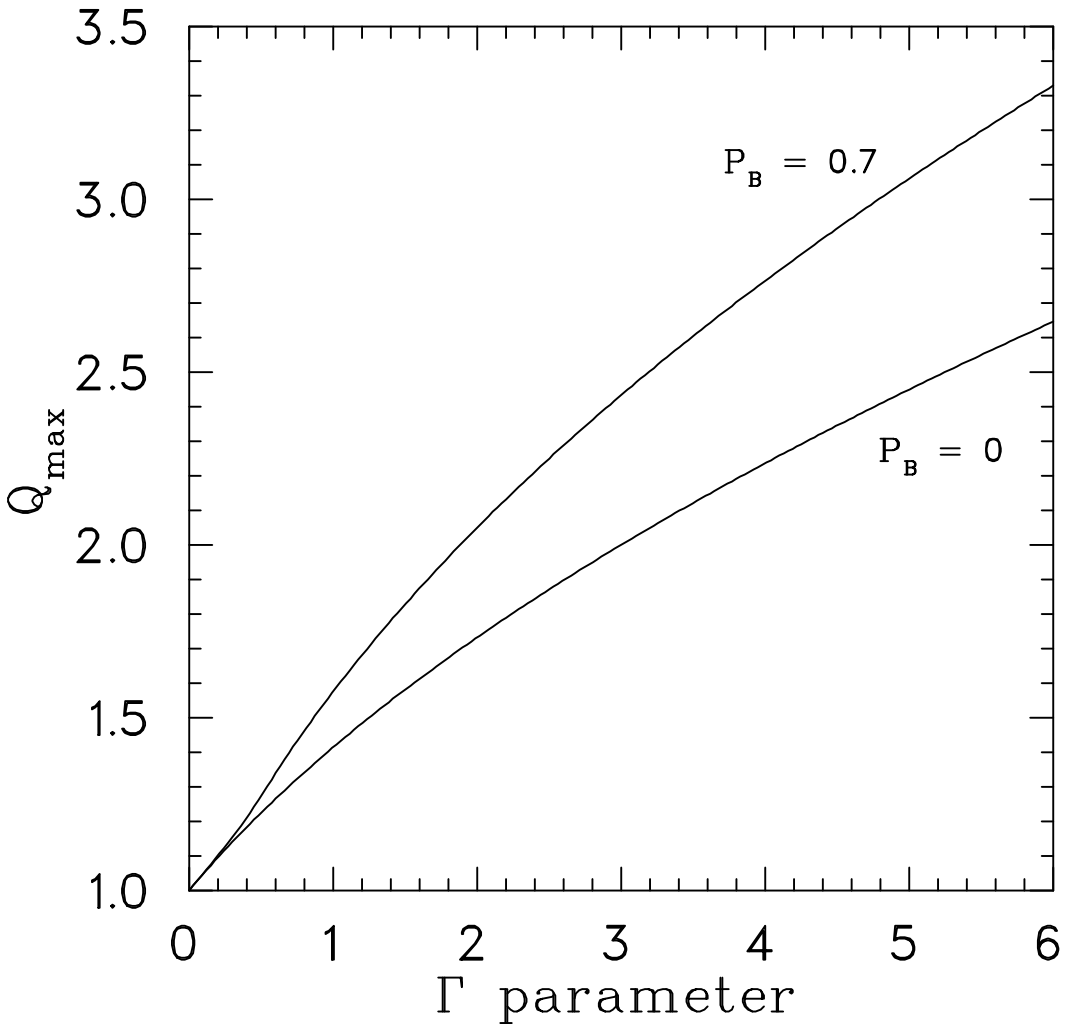

Fig. 10

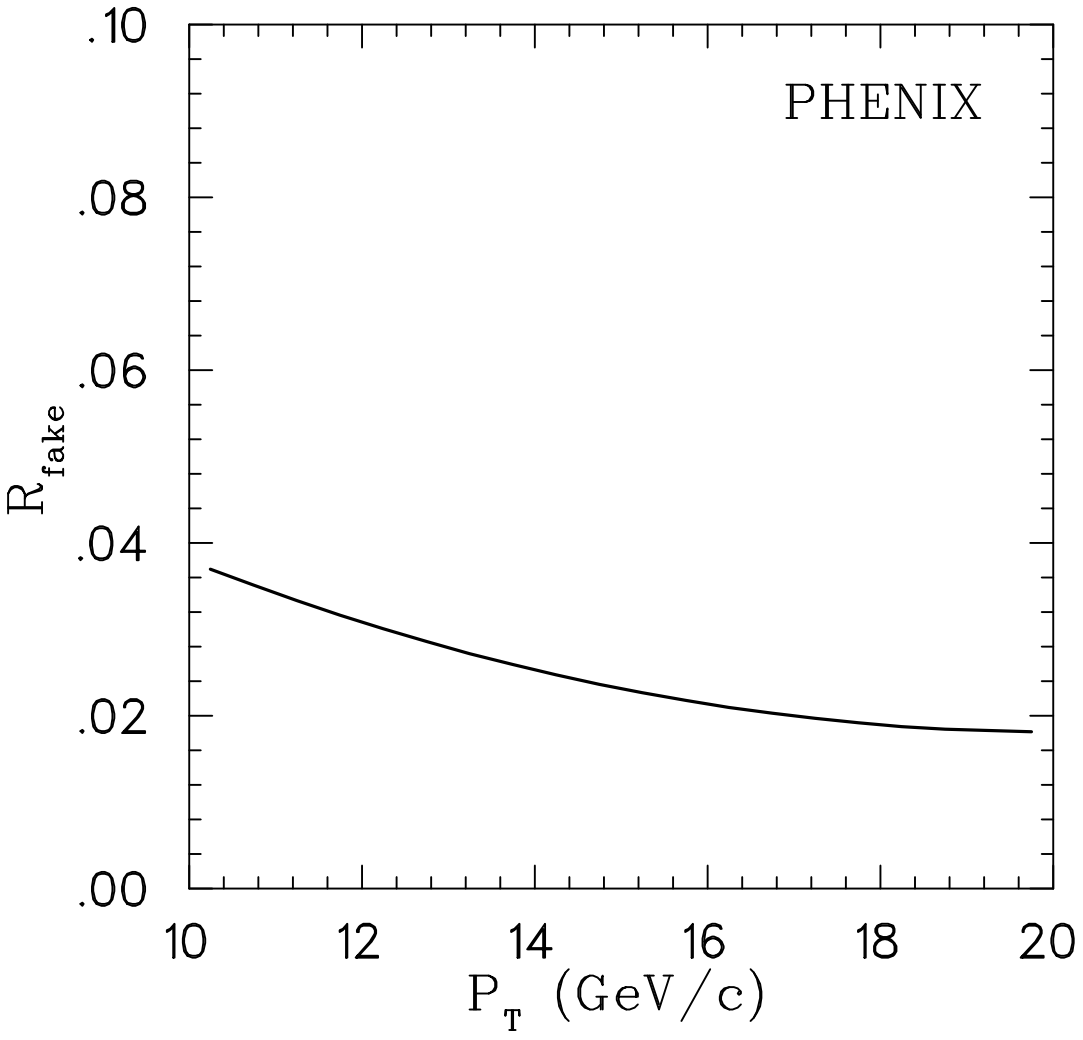

Fig. 11

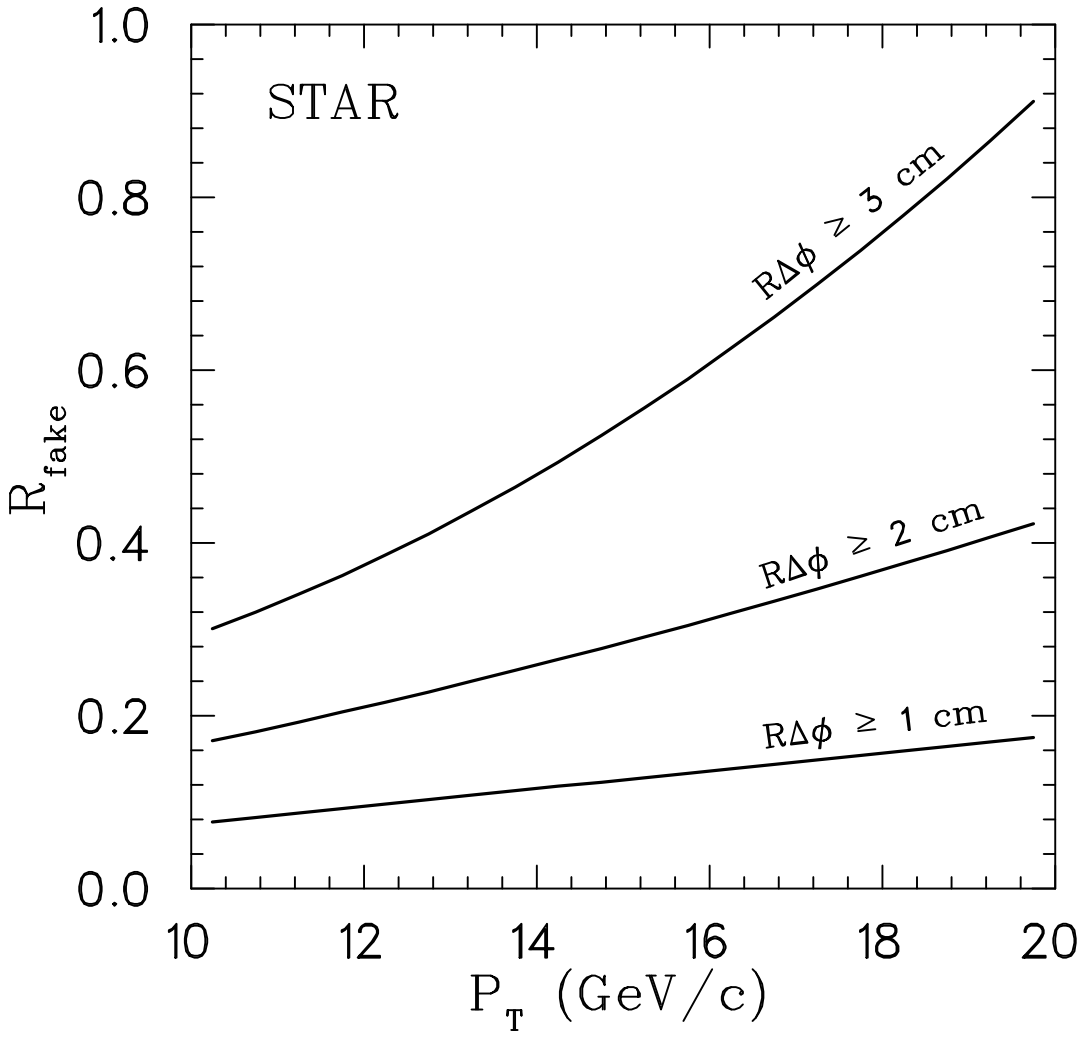
STAR
$R\Delta\phi \geq 3$ cm
$R\Delta\phi \geq 2$ cm
$R\Delta\phi \geq 1$ cm
R_{fake}
P_T (GeV/c)
1.0
0.8
0.6
0.4
0.2
0.0
10
12
14
16
18
20

Fig. 12

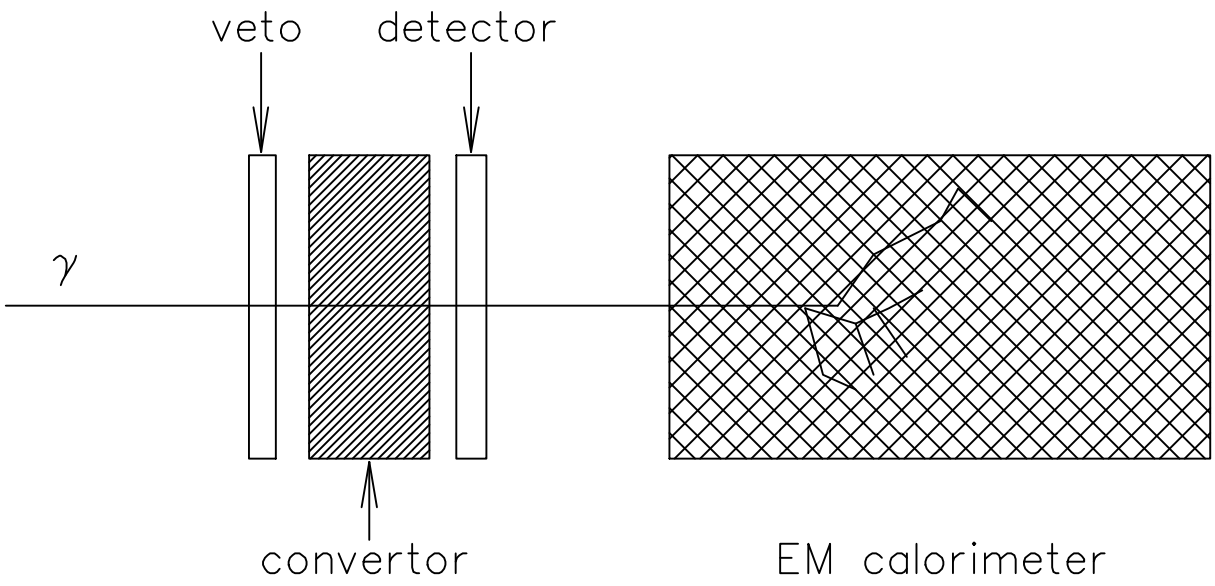
Preshower/Calorimeter layout
veto
detector
γ
convertor
EM calorimeter

Fig. 13

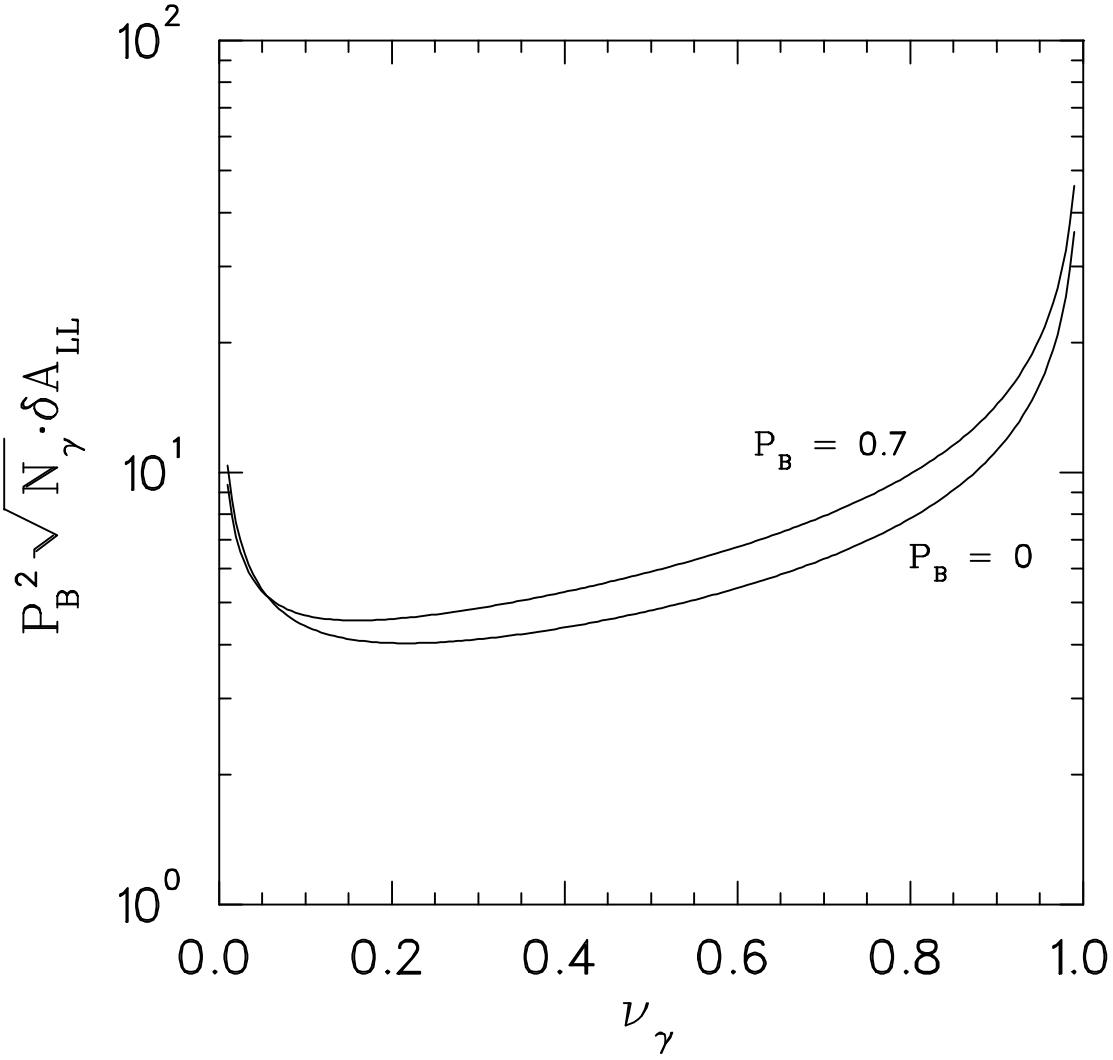
10^2
10^1
10^0
$P_B^2\sqrt{N_\gamma}\cdot\delta A_{LL}$
$P_B = 0.7$
$P_B = 0$
0.0
0.2
0.4
0.6
0.8
1.0
ν_γ

Fig. 14

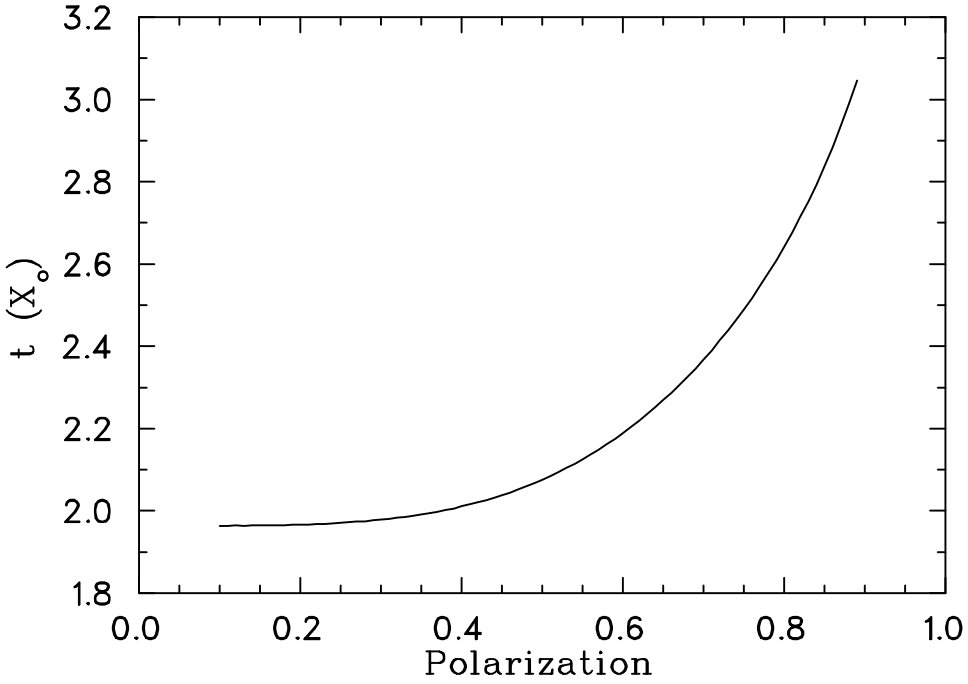
3.2
3.0
2.8
2.6
2.4
2.2
2.0
1.8
t (X$_o$)
0.0
0.2
0.4
0.6
0.8
1.0
Polarization

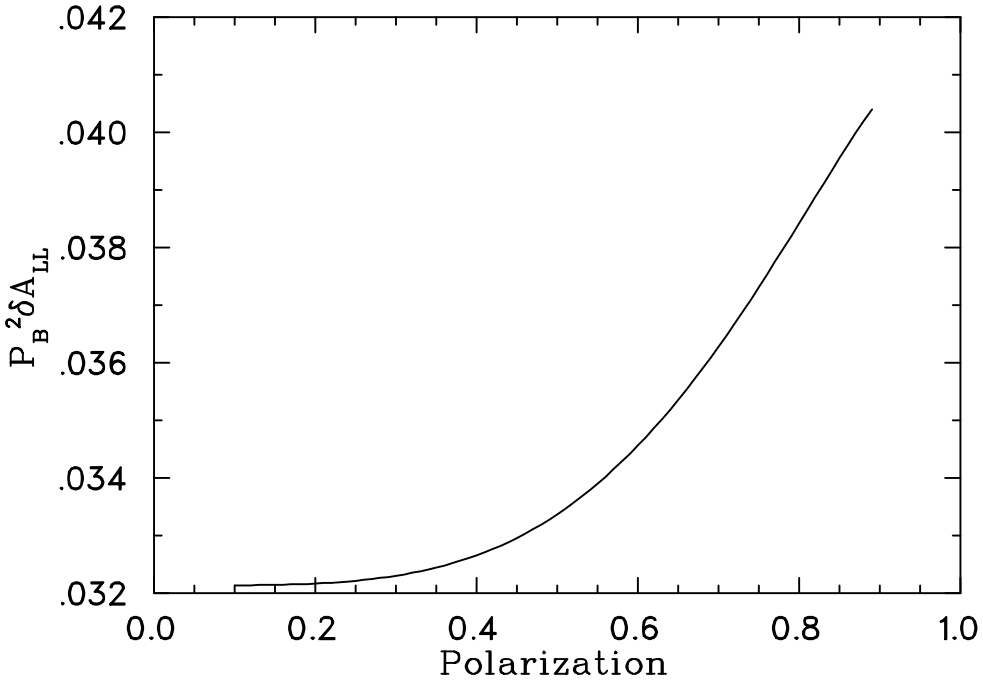
.042
.040
.038
.036
.034
.032
$P_B^2 \delta A_{LL}$
0.0
0.2
0.4
0.6
0.8
1.0
Polarization

Fig. 15

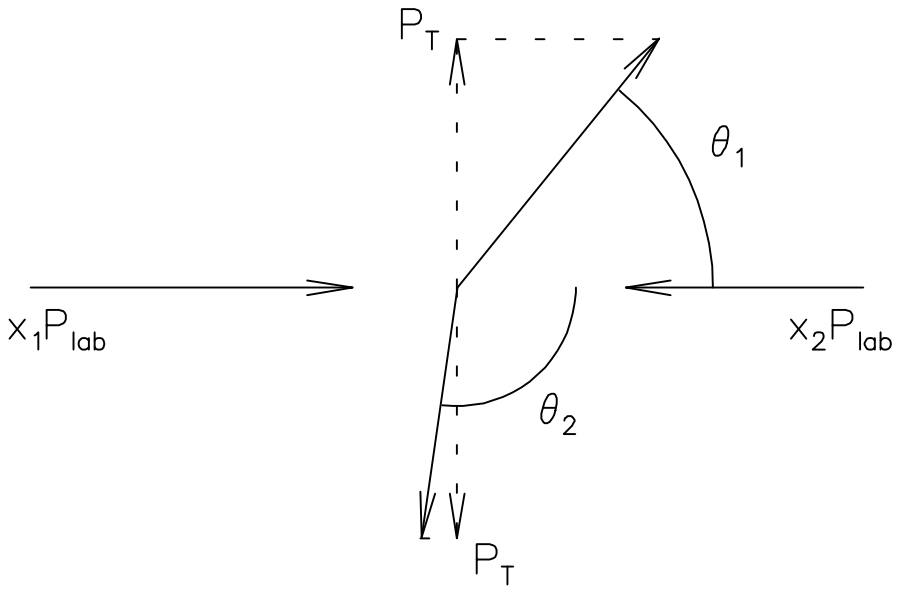

Fig. 16

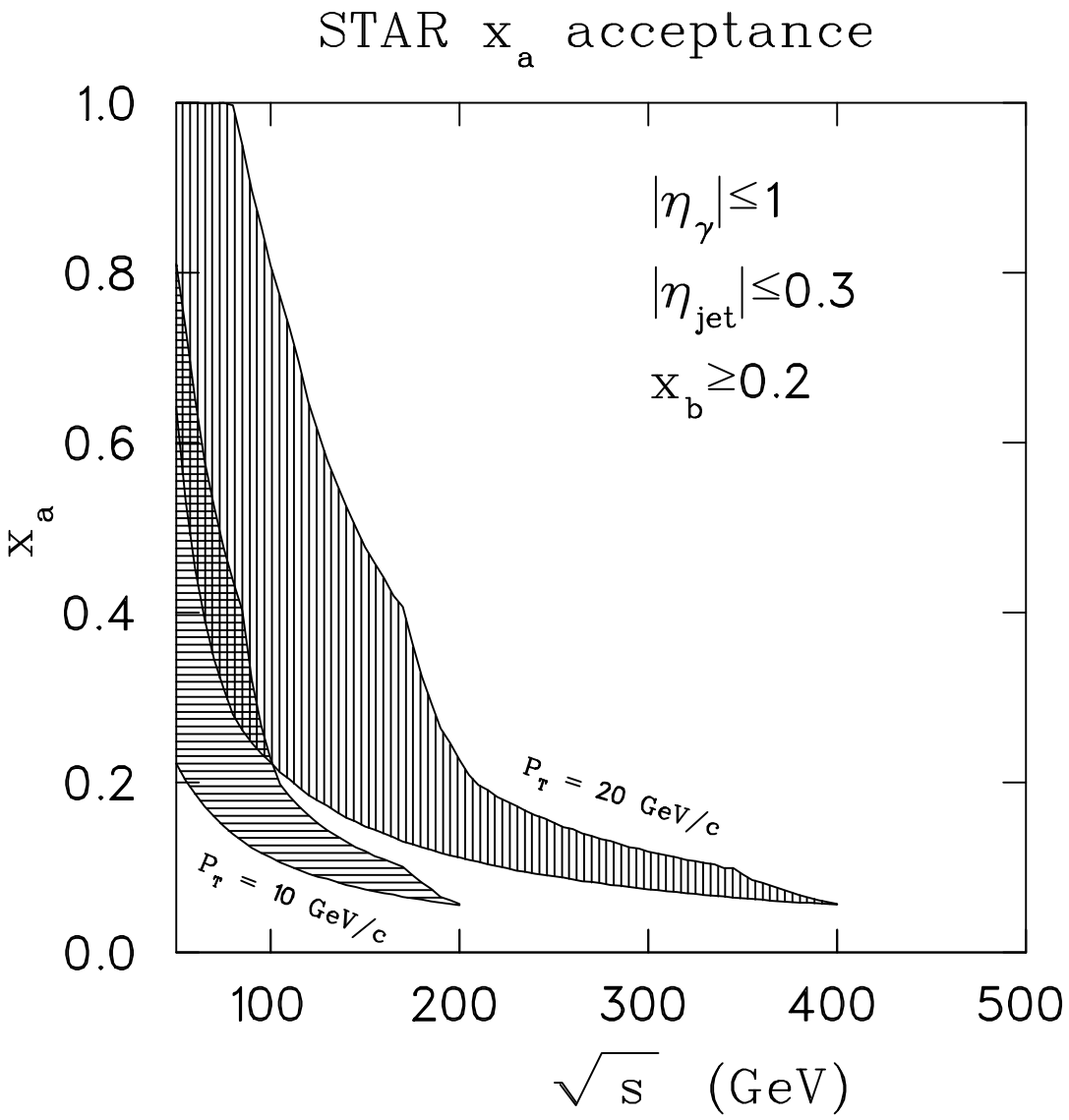
STAR x_a acceptance
$|\eta_\gamma| \leq 1$
$|\eta_{jet}| \leq 0.3$
$x_b \geq 0.2$
P_T = 20 GeV/c
P_T = 10 GeV/c
X_a
1.0
0.8
0.6
0.4
0.2
0.0
100
200
300
400
500
$\sqrt{s}$ (GeV)

Fig. 17

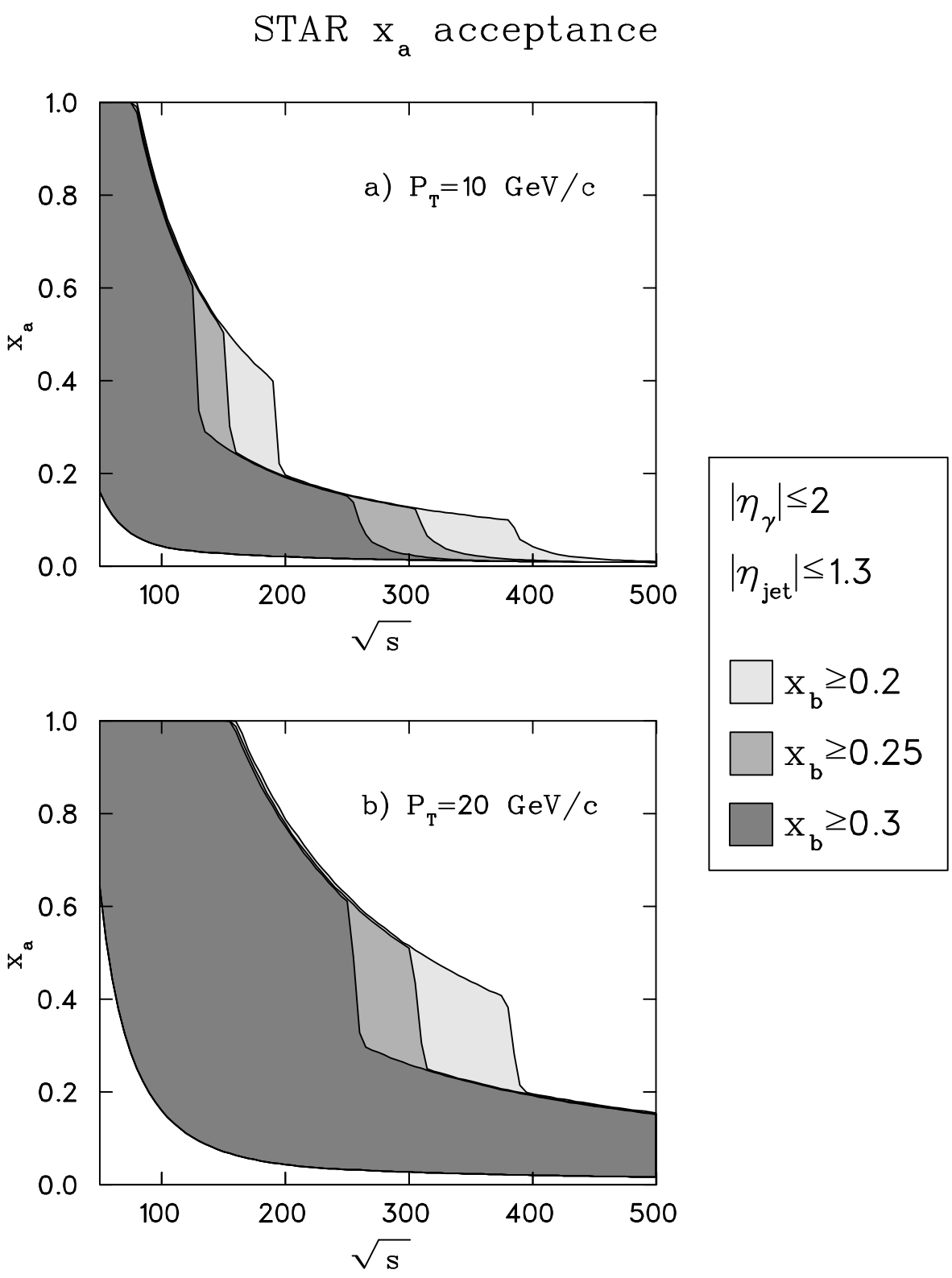
STAR x_a acceptance
a) P_T=10 GeV/c
b) P_T=20 GeV/c
x_a
$\sqrt{s}$
1.0
0.8
0.6
0.4
0.2
0.0
100
200
300
400
500
$|\eta_\gamma|\leq 2$
$|\eta_{jet}|\leq 1.3$
$x_b\geq 0.2$
$x_b\geq 0.25$
$x_b\geq 0.3$

Fig. 18

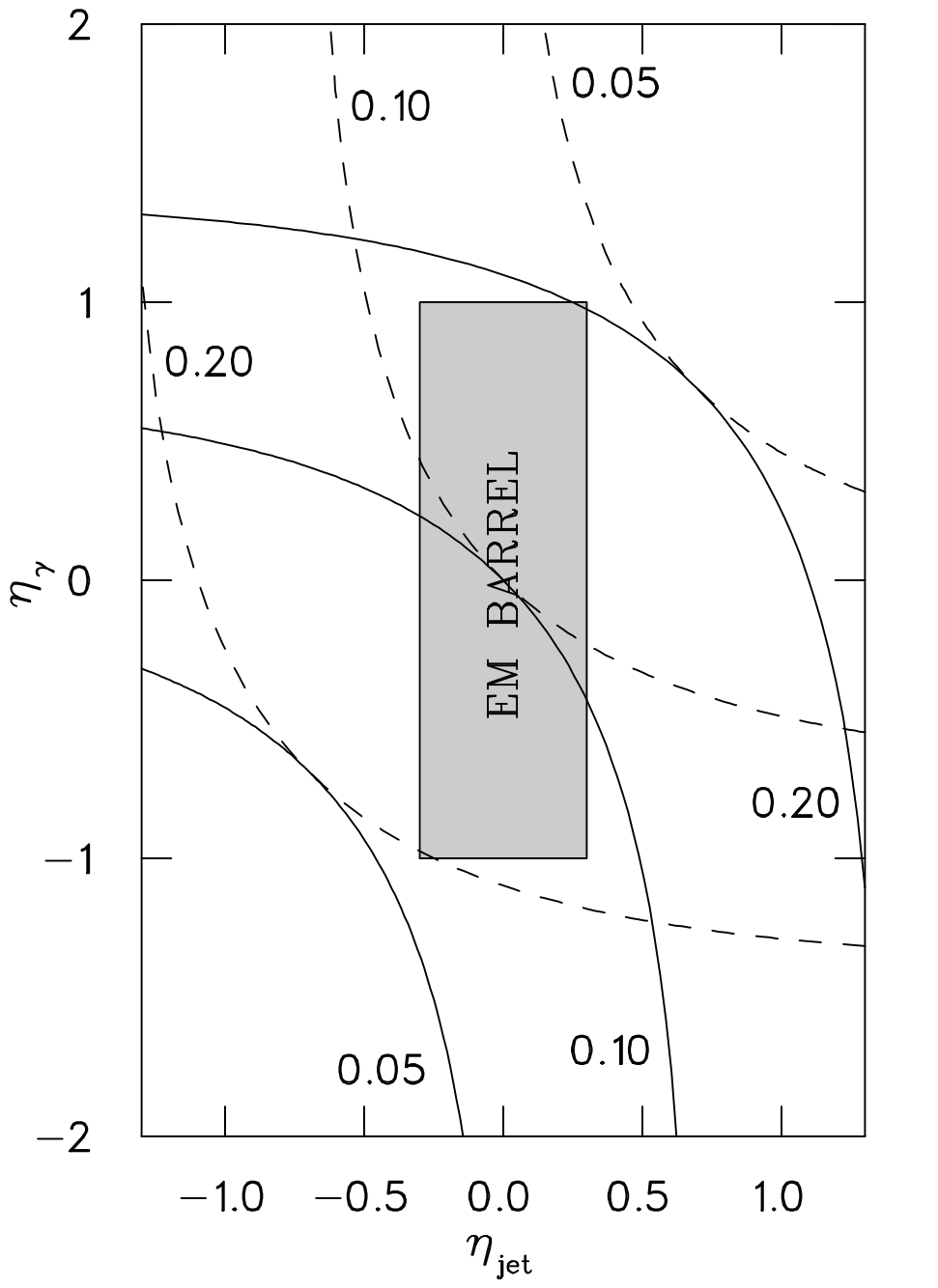
STAR x_1 and x_2 coverage for x_T=0.1
2
1
0
−1
−2
η_γ
−1.0
−0.5
0.0
0.5
1.0
η_{jet}
0.10
0.05
0.20
EM BARREL
0.20
0.05
0.10

Fig. 19

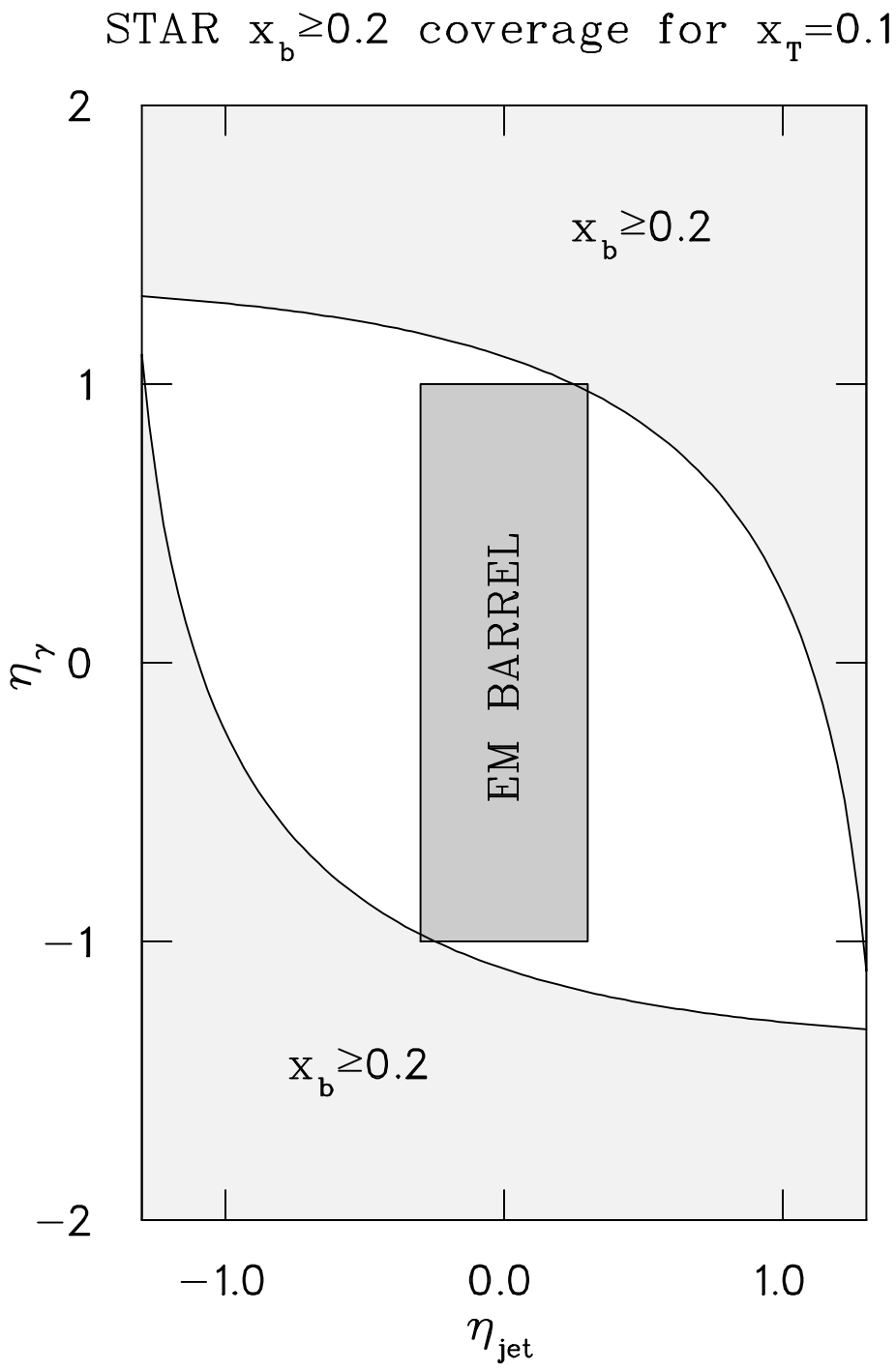
STAR $x_b \geq 0.2$ coverage for $x_T = 0.1$
$x_b \geq 0.2$
EM BARREL
$x_b \geq 0.2$
2
1
0
−1
−2
η_γ
−1.0
0.0
1.0
η_{jet}

Fig. 20

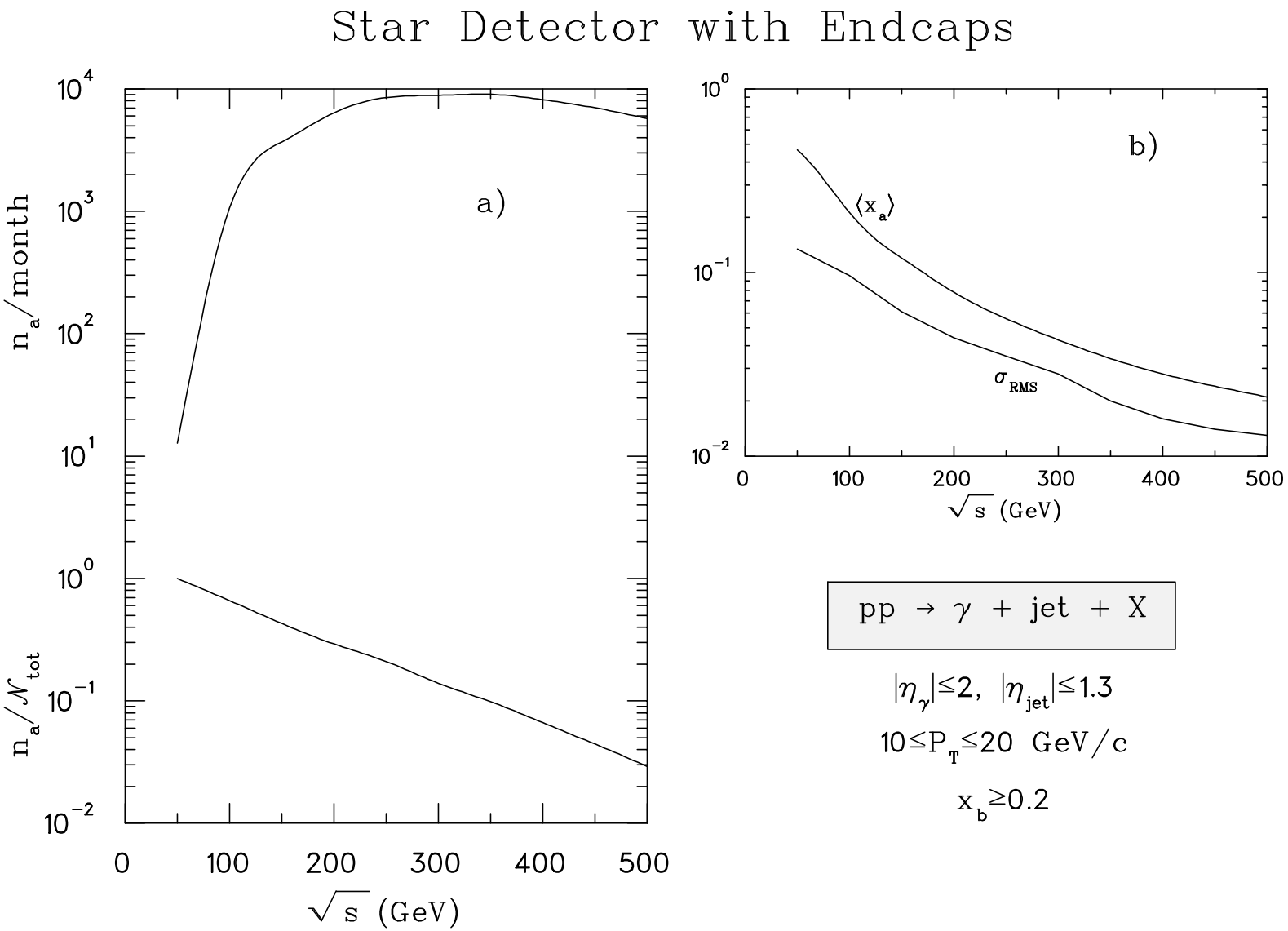
Star Detector with Endcaps
a)
b)
n_a/month
$n_a/\mathcal{N}_{tot}$
$\sqrt{s}$ (GeV)
$\langle x_a \rangle$
σ_{RMS}
pp → γ + jet + X
$|\eta_\gamma| \leq 2$, $|\eta_{jet}| \leq 1.3$
$10 \leq P_T \leq 20$ GeV/c
$x_b \geq 0.2$

Fig. 21

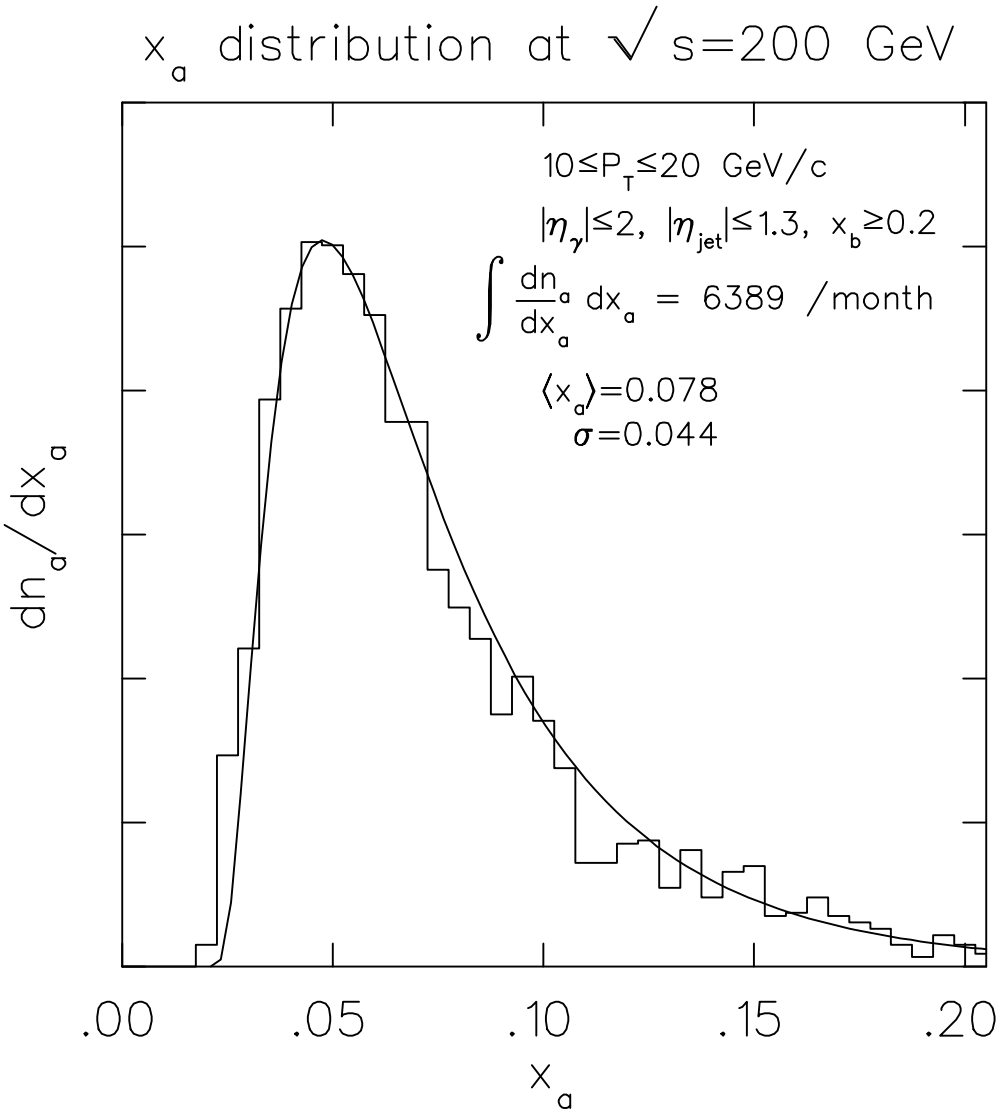
x_a distribution at $\sqrt{s}$=200 GeV
$10 \le P_T \le 20$ GeV/c
$|\eta_\gamma| \le 2$, $|\eta_{jet}| \le 1.3$, $x_b \ge 0.2$
$\int \frac{dn_a}{dx_a} dx_a$ = 6389 /month
$\langle x_a \rangle$=0.078
σ=0.044
dn_a/dx_a
.00
.05
.10
.15
.20
x_a

Fig. 22